



In-host evolution of *Yersinia enterocolitica* during a chronic human infection

Received: 15 July 2024

Accepted: 4 June 2025

Published online: 01 July 2025

Check for updates

Cyril Savin ^{1,2,3,14}✉, Pierre Lê-Bury ^{1,3,4,14}, Julien Guglielmini ⁵, Thibaut Douché ⁶, Guillem Mas Fiol ^{1,3}, Rodolphe Buzelé ^{7,8,13}, Cécile Le Brun ⁷, Frédéric Bastides ⁸, Maud François ⁹, Béatrice Birmelé ⁹, Laura Guichard ^{1,2}, Julien Madej ^{1,2}, Rémi Beau ^{1,2}, Nicolas Cabanel ^{1,2}, Laurent Doret ^{4,10,11}, Mariette Matondo ⁶, Olivier Dussurget ^{1,3}, Elisabeth Carniel ^{1,2}, Philippe Lanotte ^{7,12,15} & Javier Pizarro-Cerdá ^{1,2,3,15}

Bacteria exhibit remarkable adaptability in response to selective pressures encountered during infection and antibiotic treatment. We characterize four *Yersinia enterocolitica* clonal isolates from successive bacteremia episodes that evolved within an elderly patient over 14 years. Their common evolution is characterized by a genome size reduction resulting in the loss of about a hundred genes and a so far undescribed deletion in the DNA gyrase gene *gyrA* conferring quinolone resistance. Third-generation cephalosporin resistance of the last isolate correlates with a truncation of OmpF in synergy with an increased production of BlaA and AmpC β -lactamases. A strong proteome remodeling of the isolates reveals a perturbed stringent response, as well as impaired metabolism which substantiate their severe growth defects in vitro, accounting for antibiotics tolerance and possibly therapeutic failure. This study documents previously unreported genetic and phenotypic changes associated with in-host adaptation of a pathogenic *Yersinia* species under antibiotic pressure.

In the past few years, genome evolution of pathogenic bacteria during chronic infection has been analyzed to unprecedented depth through whole-genome sequencing-based longitudinal studies of clinical isolates¹. Mainly focusing on cystic fibrosis-associated bacteria such as *Staphylococcus aureus*, *Pseudomonas aeruginosa*, and *Burkholderia* species but also encompassing other important pathogens such as

Mycobacterium tuberculosis, *Salmonella enterica*, *Helicobacter pylori* or *Enterococcus* species, these studies unraveled shared within-host evolution mechanisms such as genome size reduction, metabolic adaptation, virulence modulation or hypermutation¹⁻³. Furthermore, longitudinal genomic studies shed light on antibiotic resistance emergence during chronic infection by the mean of various evolutive

¹Institut Pasteur, Université Paris Cité, Yersinia Research Unit, Paris, France. ²Institut Pasteur, Université Paris Cité, Yersinia National Reference Laboratory, Paris, France. ³Institut Pasteur, Université Paris Cité, WHO Collaborating Research and Reference Centre for Plague FRA-146, Paris, France. ⁴Université Paris-Saclay, Inserm, CEA, Center for Immunology of Viral, Auto-immune, Hematological and Bacterial diseases (IMVA-HB/IDMIT/UMRS1184), Fontenay-aux-Roses & Le Kremlin-Bicêtre, France. ⁵Institut Pasteur, Université Paris Cité, CNRS UMR 3756, Biostatistics and Bioinformatics Hub, Paris, France. ⁶Institut Pasteur, Université Paris Cité, CNRS UAR2024, Proteomic Platform, Mass Spectrometry for Biology Unit, Paris, France. ⁷Service de Bactériologie-Virologie, CHRU de Tours, Tours, France. ⁸Service de Médecine Interne et des Maladies Infectieuses, CHRU de Tours, Tours, France. ⁹Service d'Hémodialyse, CHRU de Tours, Tours, France. ¹⁰Centre Hospitalier Universitaire de Hôpital Bicêtre, Université Paris Saclay, AP-HP, Service de Bactériologie-Hygiène, Le Kremlin-Bicêtre, France. ¹¹Centre National de Référence Associé de la Résistance aux Antibiotiques, Le Kremlin-Bicêtre, France. ¹²ISP, INRA, Université de Tours, UMR1282, Nouzilly, France. ¹³Present address: Service de Médecine Interne, CH Yves Le Foll, Saint Brieuc, France. ¹⁴These authors contributed equally: Cyril Savin, Pierre Lê-Bury. ¹⁵These authors jointly supervised this work: Javier Pizarro-Cerdá, Philippe Lanotte. e-mail: cyril.savin@pasteur.fr; javier.pizarro-cerda@pasteur.fr

or ecological mechanisms^{2,4}. In contrast, in-host evolution of antibiotics tolerance that contributes to this emergence⁵ is still poorly understood⁶⁻⁸.

In-host evolution has not been reported for infections associated with *Yersinia* spp. Yersinioses include fulminant infections such as plague caused by *Yersinia pestis*, as well as mild or severe enteritis caused by *Yersinia pseudotuberculosis* or *Yersinia enterocolitica* (Ye)⁹. The latter represents the third most common cause of enteritis from bacterial origin in temperate and cold countries¹⁰. Systemic Ye infections occur mostly in elderly patients with underlying disorders such as diabetes, iron overload, or cirrhosis¹¹.

Persistent Ye infections in patients causing relapses for several years have been reported¹², but the potential genetic relationships between the isolated strains was not determined.

In this work, we report a previously undescribed in-host evolution of a pathogenic *Yersinia* species in a patient presenting iterative episodes of bacteremia over 14 years despite long-term antibiotics

treatments. Analyses of 4 clinical isolates reveal genome size reduction, impaired metabolism and increased doubling time, hallmark of antibiotics tolerance, in the latest isolates. This tolerance likely paves the way to quinolone resistance acquisition via a previously undescribed mutation in the *gyrA* gene encoding the DNA gyrase A subunit, and, ultimately, to OmpF- and β -lactamase-mediated ceftriaxone resistance acquisition in the latest isolate, leading to therapeutic failure.

Results

Case description

An elderly patient presented with an atrioventricular block that led to a pacemaker implantation in September 1998. In December 1999, the patient had a first septicemic episode resulting in the isolation of a Ye strain (Ye.1) (Fig. 1a). She received ceftriaxone and netilmicin treatment for 4 weeks and recovered. In February 2000, the patient experienced a second episode of bacteremia with isolation of another

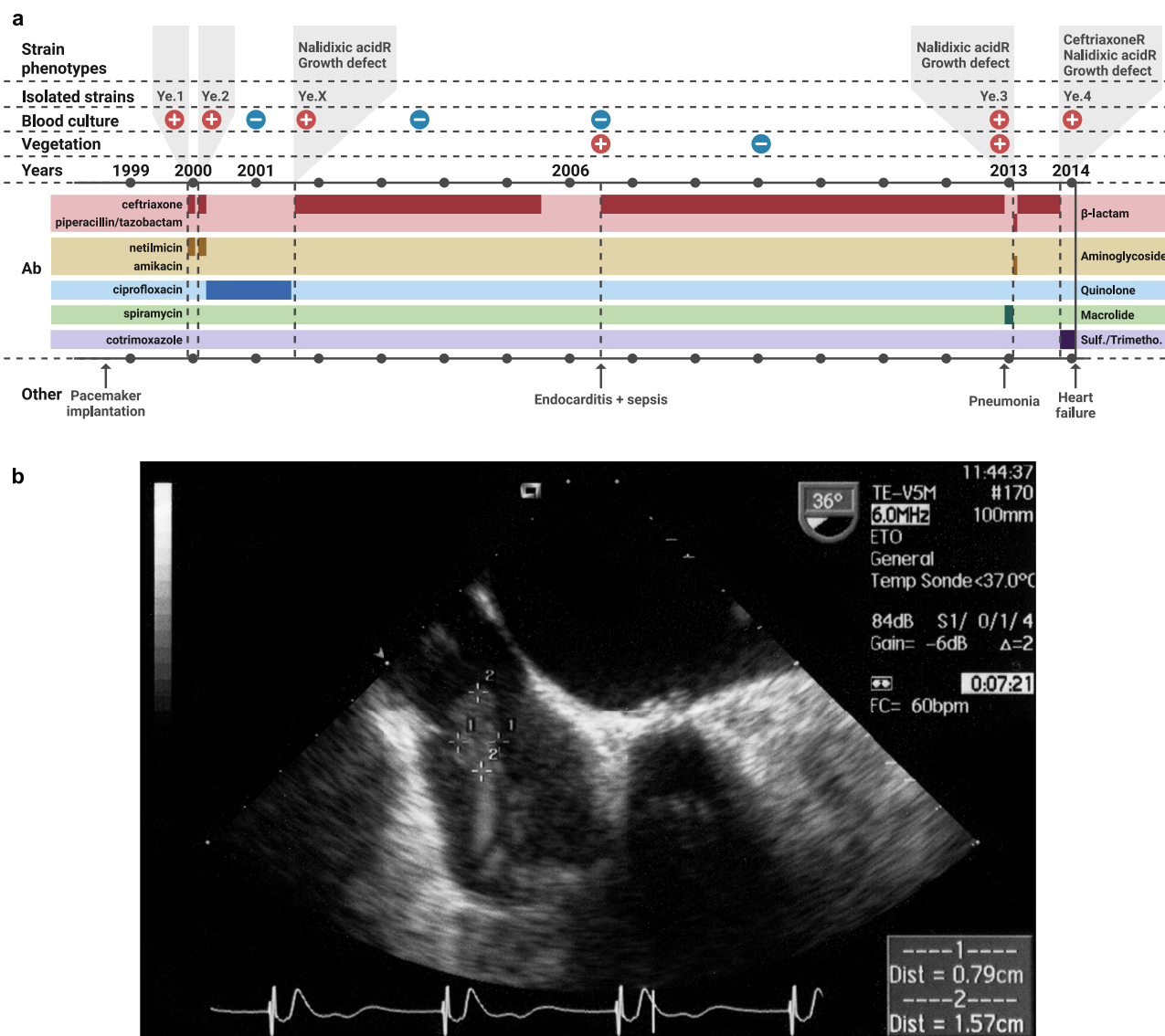


Fig. 1 | Clinical case description. **a** Clinical case description of Ye chronic infection. Positive and negative symbols reflect the blood culture results, or the observation of vegetations on the pacemaker atrial lead. Periods of antibiotics treatment are shown in a darker color on the chronograph, with the associated treatment names on the left and antibiotic classes on the right. Ab: antibiotics. CeftriaxoneR: resistant to ceftriaxone. Nalidixic acidR: resistant to nalidixic acid.

Sulf: sulfonamide. Trimetho: Trimethoprim. Created in BioRender. Lê-bury, P. (2025) <https://BioRender.com/7nptf49> **b** Vegetation on pacemaker lead. Transthoracic echocardiography performed July 27th, 2006, showing large vegetations on the pacemaker lead in the right atrium. Vegetations formed a sheath around the electrode, measuring 1.6 cm by 0.8 cm.

Ye strain (Ye.2). She was treated with the same antibiotics for four weeks, followed by 18 months of ciprofloxacin therapy (until July 2001), during which monthly blood cultures were negative. A third bacteremia occurred in August 2001 with isolation of a third *Ye* (Ye.X, not kept in collection) that showed a decreased growth rate, and was resistant to nalidixic acid but susceptible to ciprofloxacin, which had been used for treatment. The patient received a long-term ceftriaxone therapy until July 2005, and monthly blood cultures were negative. In June 2006, the patient was hospitalized for a sepsis but had a negative blood culture. For the first time, echocardiography evidenced vegetations on the pacemaker atrial lead, suggesting endocarditis due to bacterial growth on the cardiac device (Fig. 1b). A 6-year ceftriaxone treatment was administered, leading to vegetation disappearance. In December 2012, the patient suffered from pneumonia, and ceftriaxone treatment was replaced by spiramycin. In January 2013, she presented with another bacteremia with isolation of a fourth *Ye* strain (Ye.3) and vegetations reappeared on the pacemaker atrial lead. Strain Ye.3, like Ye.X, was resistant to nalidixic acid and showed a severe growth defect. The patient was treated with piperacillin/tazobactam/amikacin for one week, followed by a 9-month ceftriaxone therapy. The patient had a last bacteremia in October 2013, during which a fifth *Ye* strain (Ye.4) was isolated. Minimum inhibitory concentration (MIC) of ceftriaxone increased from 0.19 mg/L (Ye.3) to 2 mg/L (Ye.4) leading to antimicrobial treatment modification with cotrimoxazole. Three months later, the patient died of heart failure.

Antibiotic susceptibility evolution upon long-term treatment

The five strains isolated during the iterative bacteremia were initially identified as *Ye* using a VITEK2 GN card. Ye.1 and Ye.2 (also referred as “early isolates”) were identified as *Ye* bioserotype 4/O:3 by phenotypical characterization; Ye.3 and Ye.4 (also referred as “late isolates”) were not characterized by these methods. A substantial increase in mid-exponential phase doubling time at 37 °C was measured, from 49 and 44 min for Ye.1 and Ye.2 to 5h38 and 4h46 for Ye.3 and Ye.4, respectively. Doubling times at 28 °C were slightly longer, with 57 min for Ye.1 and Ye.2, 6h49 for Ye.3 and 5h28 for Ye.4 (Supplementary Fig. 1).

After isolation of the four strains, we parallelly assessed the susceptibility of Ye.1 to Ye.4 to single antibiotics or to antibiotic combinations (Abs) by disk diffusion assay (33 Abs) and Etest (10 Abs) (Table 1). All strains were resistant to the penicillins amoxicillin and ticarcillin. Ye.1 and Ye.2 were resistant to 1st-generation cephalosporin and they were susceptible to all other tested antibiotics, as usually observed for *Ye* bioserotype 4/O:3, although Ye.2 showed a small resistance increase to several β-lactams and netilmicin, the aminoglycoside (AG) which was administered in combination with the 3rd-generation cephalosporin (C3G) ceftriaxone between Ye.1 and Ye.2 isolation. Ye.3 and Ye.4 acquired a resistance to the quinolone nalidixic acid, as observed with Ye.X, and an AG MIC decrease was observed compared to the early isolates Ye.1 and Ye.2. Furthermore, Ye.4 was fully resistant to the C3G ceftriaxone as well as the 2nd-generation cephalosporin (C2G) cefoxitin, and was slightly more resistant than Ye.3 to piperacillin-tazobactam, the combination of a penicillin and a β-lactamase inhibitor administered before ceftriaxone between Ye.3 and Ye.4 isolation.

To better understand how the late isolates survived long-term ciprofloxacin treatment despite absence of detectable resistance, we measured the killing kinetics when bacteria were exposed to various ciprofloxacin concentration to assess tolerance. Of note, as the latest isolates could not grow in Mueller-Hinton (MH) broth, we measured the survival in Lysogeny Broth (LB). Interestingly, while MIC measured by Etest on the standard MH agar were fairly constant between the four isolates, we observed an increasing resistance from early to late isolates when MIC were measured in LB broth by microdilution assay (Table 1). However, LB is a complex and unstandardized

medium for MIC determination, limiting interpretation of these differences. To evaluate killing kinetics, a range of ciprofloxacin concentrations was first tested on the most sensitive isolate Ye.1 (Supplementary Fig. 2a, b). Two concentrations were then chosen to assess the killing kinetics of the four isolates with enough sensitivity. The highest concentration (0.25 µg/mL) was 2- to 16-fold the LB MIC of Ye.1, Ye.2 and Ye.3, although it was below the Ye.4 MIC measured in LB. At this concentration, Ye.1 and Ye.2 were killed within the first 3 h, while Ye.3 displayed a slower killing rate and could still be detected after 25 h of incubation (Fig. 2, Supplementary Fig. 2c-j). At a lowest concentration (0.0625 µg/mL), Ye.2 showed a better survival than Ye.1 (Fig. 2i) after 3 h of incubation. Overall, these results show an increase in tolerance to ciprofloxacin from isolates Ye.1 to Ye.3.

Genomic evolution during the chronic *Ye* infection

Taxonomic assignment of the 4 isolated strains was obtained based on a core-genome multi-locus sequence typing (cgMLST) with 500 core genes using whole-genome de novo sequences, confirming that strains Ye.1 to Ye.4 belong to the *Ye* genotype 4, corresponding to bioserotype 4/O:3. To investigate whether the multiple infection episodes were independent or due to a chronic colonization by a unique evolving bacterial strain, we studied the genetic relatedness of strains Ye.1 to Ye.4 by a core-genome single-nucleotide polymorphism (SNP) analysis, with inclusion of 259 additional *Ye* biotype 4 strains isolated between 1963 and 2016 (Supplementary Data 1). The phylogenetic tree reconstruction based on analysis of 4,738 SNPs showed that Ye.1 to Ye.4 were closely related and formed a unique clade separated from other *Ye* strains, and that the late isolates belonged to a long branch, suggesting an unusual accumulation of SNPs (Fig. 3a). Using Bayesian phylogenetic inference, we estimated the substitution rate for the four strains to 10⁻⁵ and 10⁻⁶ substitutions per site per year (Supplementary Fig. 3a), which is comparable to the rates observed in other in-host evolving bacterial strains¹. These results strongly suggest that the patient suffered from a chronic infection due to a unique evolving *Ye* 4/O:3 strain.

We next analyzed the molecular events that characterized the in-host evolution of Ye.1 to Ye.4. Genomic comparison and pan-genome phylogenetic analysis did not evidence any gene acquisition or small insertion/deletion events that were common and specific to the four *Ye* isolates. Ye.1 (isolated in December 1999) and Ye.2 (isolated in February 2000) were identical except for the loss in Ye.1 of a 1.5 kb region (between nucleotides 4,282,424 and 4,283,952 from the Y11 reference genome), indicating that detectable genetic divergence occurred within the first months of infection. Using the phylogenetic tree, we selected 4 other strains with the shortest genetic distance to the 4 *Ye* clinical isolates and investigated the putative presence of a temporal signal. Due to the unusual accumulation of SNPs, Ye.3 and Ye.4 represented outliers and were excluded from the analysis. We found evidence of a temporal signal present in the evolution of the 6 other strains (Supplementary Fig. 3b). The use of the least-squares dating tool (<https://lsdating.pasteur.fr>) estimated the closest internal node for Ye.1 and Ye.2 in October 1999, suggesting that the patient was contaminated at least two months before the first bacteremic episode (Fig. 3b). The closest internal node for Ye.3 (isolated in January 2013) and Ye.4 (isolated in October 2013) was estimated to be January 2011 (Fig. 3b). Their common ancestor accumulated 285 SNPs before diverging into Ye.3 and Ye.4, which since accumulated 31 and 52 additional SNPs, respectively (Fig. 3a, Supplementary Data 2). 140 genes containing mutations vertically acquired from their common ancestor (synapomorphies) were identified in the Ye.3 and Ye.4 genomes, including the *gyrA* gene (see below and Supplementary Data 3). Ye.3 and Ye.4 shared three identical large deletions: a 2-gene deletion of 2.5 kb, which additionally led to the truncation of the *dksA* gene (see below), a 9-gene deletion of 9.9 kb, and a 28-gene deletion of 32.7 kb (Supplementary Data 4). These strains also shared 41 small insertions/

Table 1 | Antibiotic susceptibility profiling of the 4 clinical isolates

Antibiogram						
Class	Subclass	Antibiotic	Ye.1	Ye.2	Ye.3	Ye.4
β-lactam	penicillin (4 G)	piperacillin-tazobactam ³	-	-	-	-
	penicillin (4 G)	piperacillin	-	r	-	-
	penicillin (4 G)	ticarcillin	R	R	R	R
	penicillin (3 G)	amoxicillin	R	R	R	R
	carbapenem	ertapenem	-	-	-	-
	penicillin	ticarcillin-clavulanate	-	-	-	-
	cephem (3 G)	ceftazidime	-	r	-	-
	cephem (2 G)	cefoxitin	-	r	-	R
	penicillin (4 G)	temocillin	-	r	-	-
	carbapenem	imipenem	-	r	-	-
	penicillin (3 G)	amoxicillin-clavulanate	-	r	-	-
	cephem (3 G)	cefotaxime	-	r	-	-
	cephem (3 G)	ceftazidime-avibactam	-	r	-	-
	carbapenem	meropenem	-	-	-	-
	monobactam	aztreonam	-	-	-	-
	cephem (4 G)	cefepime	-	-	-	-
	cephem (3 G)	moxalactam	-	r	-	-
	penicillin	mecillinam	-	r	-	-
	cephem (5 G)	ceftolozan-tazobactam	-	r	-	-
	cephem	cefiderocol	-	r	-	-
quinolone	quinolone	nalidixic acid	-	-	R	R
	fluoroquinolone	levofloxacin	-	-	-	-
	fluoroquinolone	ciprofloxacin ²	-	-	-	-
tetracycline		tigecycline	-	-	-	-
fosfomycin		fosfomycin	-	-	-	-
nitrofuran		nitrofurantoin	-	-	-	-
sulfonamide-trimethoprime		sulfamethoxazole-trimethoprim	-	-	-	-
amphenicol		chloramphenicol	-	-	-	-
polymyxin		colistin	-	-	-	-
aminoglycosides		gentamicin	-	-	-	-
		amikacin ³	-	-	-	-
		tobramycin	-	-	-	-
		netilmicin ¹²	-	r	-	-
MIC						
Class	Subclass	Antibiotic	Ye.1	Ye.2	Ye.3	Ye.4
β-lactam	cephem (3 G)	ceftriaxone ¹²³	0.047	0.094	0.094	> 256
	cephem (2 G)	cefoxitin	4	12	12	> 256
	penicillin (4 G)	piperacillin-tazobactam ³	0.094	0.25	<0.016	0.094
aminoglycosides and aminoglycosides-like		netilmicin ¹²	0.75	3	0.064	0.064
		amikacin ³	3	3	2	1
		tobramycin	1	1	0.094	0.094
		gentamicin	0.5	1	0.094	0.094
		spectinomycin	12	24	0.094	0.094
Quinolone	fluoroquinolone	ciprofloxacin ² (Etest - MH)	0.008	0.012	0.002	0.032
	fluoroquinolone	ciprofloxacin ² (microdilution - LB)	0.015	0.03	0.125	0.5
	fluoroquinolone	levofloxacin	0.032	0.032	0.008	0.032

¹Administered treatment between Ye.1 and Ye.2 isolation.²Administered treatment between Ye.2 and Ye.3 isolation.³Administered treatment between Ye.3 and Ye.4 isolation.

3 G: 3rd generation. 4 G: 4th generation. 5 G: 5th generation. -: susceptible. R: resistance. r: increased resistance compared to previous strain. MH: Mueller-Hinton. LB: Lysogeny Broth. Source data are provided as a Source Data file.

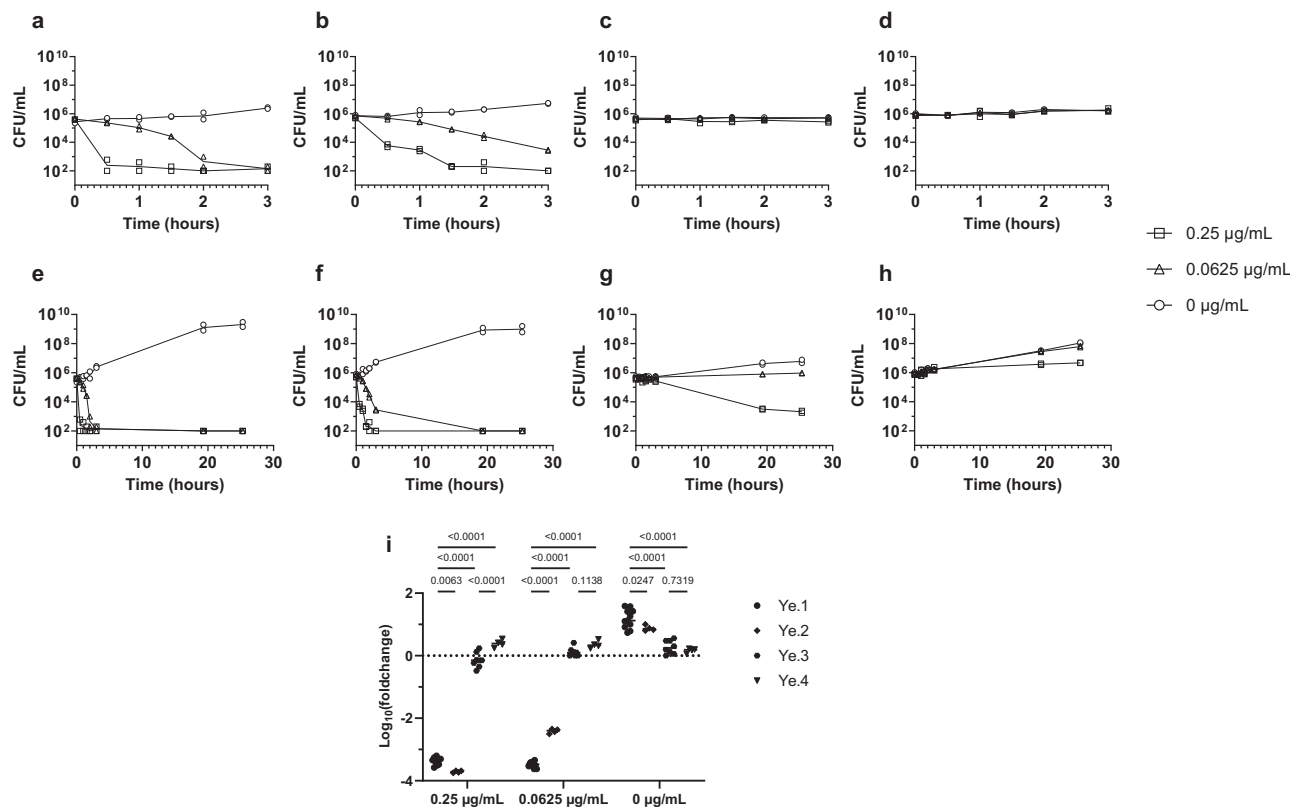


Fig. 2 | Ye survival curves during ciprofloxacin exposure. Survival curve until: a–d 3 h; e–h 25 h for: a, e Ye.1; b, f Ye.2; c, g Ye.3; d, h Ye.4 exposed to various concentration of ciprofloxacin at 37 °C in LB. The individual values of $n = 2$ replicated wells are plotted and the line represents the geometric mean. The limit of detection is at 100 colony forming units (CFU)/mL. A duplicate experiment can be found in Supplementary Fig. 2. i Survival of the four isolates after 3 h of incubation. Plotted are $\log_{10}(\text{foldchange})$ of CFUs at 3 h compared to inoculum. Data comes

from $n = 11$ replicated wells from 4 independent experiments (Ye.1), $n = 4$ replicated wells from 2 independent experiments (Ye.2), $n = 8$ replicated wells from 3 independent experiments (Ye.3), and $n = 4$ replicated wells from 2 independent experiments (Ye.4). Statistics are computed by two-way ANOVA with Tukey multiple comparisons test (non-directional) on the $\log_{10}(\text{foldchange})$ and only selected p value are plotted for clarity. Source data are provided as a Source Data file.

deletions (Supplementary Data 4), overlapping with the previous synapomorphies. While 6 genes did not exhibit any frameshift, 35 genes displayed a mutation potentially leading to a truncated form of their product. Out of the 74 truncated genes and genes in deleted regions, 64 belonged to Ye core-genome (defined as genes present in more than 95% Ye genomes) while 10 belonged to the remaining accessory genome. They were found to be involved in essential physiological functions such as transcription, translation, replication, respiration, division, and carbohydrate and iron metabolisms (Supplementary Data 4). We identified several mutated genes potentially leading to truncated or modified products which had already been shown to be involved in antibiotics resistance or evolvability such as the DNA gyrase subunit A gene *gyrA*, the RNA polymerase-binding transcription factor gene *dksA*, the outer membrane porin gene *ompF* or the transcription-coupled repair (TCR) factor gene *mfd*.

Genetic basis of antibiotics resistance and susceptibility

The genetic basis of antibiotic resistance was investigated upon bacterial genome sequencing. Comparison of *gyrA* sequences of Ye.1 to Ye.4 with those of the reference strains Y11 and IP38477, which are susceptible to nalidixic acid, showed that Ye.3 and Ye.4 displayed the same 3-nucleotide deletion at positions 245–247 in the quinolone resistance-determining region (QRDR) of *gyrA* (Supplementary Fig. 4a). This so far undescribed deletion leads to replacement of aspartic acid 82 and serine 83 with a unique glycine without any frameshift (Supplementary Fig. 4b). Ye.4 additionally showed a nucleotide substitution leading to the substitution of aspartic acid 87 with an asparagine, a mutation already known to confer nalidixic acid

resistance^{13,14}. To further investigate the impact of these mutations, we introduced the Ye.3 3-nucleotide deletion in the Ye.1 genetic background (Ye.1-*gyrA*^{Ye.3}) as well as the D87N substitution present in Ye.4 in the Ye.1 genetic background (Ye.1-*gyrA*^{D87N}), and we verified by whole genome sequencing (WGS) the absence of other mutations in genes known to confer quinolone resistance. As expected, Ye.1-*gyrA*^{D87N} was resistant to nalidixic acid. Due to the difficulty in removing an amino acid from an essential gene like *gyrA*, we could only obtain a single Ye.1-*gyrA*^{Ye.3} clone, in which we observed 2 additional SNPs (Supplementary Table 1) along the expected *gyrA* mutation. By assessing the antibiotic susceptibility profiles with the same Abs as before, we observed that the Ye.1-*gyrA*^{Ye.3} clone was resistant to nalidixic acid and showed a MIC increase for the fluoroquinolones ciprofloxacin and levofloxacin (0.006 to 0.047 and 0.023 to 0.125 µg/mL respectively), but not antibiotics from other classes (Table 2). Despite the presence of two additional mutations involving genes not previously associated with nalidixic acid resistance, we thus expect this *gyrA*^{Ye.3} mutation to be the genetic basis of the quinolone resistance in Ye.3 and Ye.4.

We also observed a nucleotide substitution which introduced a stop codon in position 78 of the Ye.4 OmpF porin, truncating the protein at one fifth of its length (Supplementary Data 2). As porin mutations are usually associated with a decreased antibiotics uptake through the outer-membrane^{15,16}, we introduced this specific SNP in the Ye.1 genetic background to assess its role in resistance to the Abs panel. The resulting Ye.1-*ompF*^{Ye.4} strain showed a substantial increase in cefotaxime MIC (6 to 24 µg/mL), a C2G highly sensitive to membrane permeability, but only a slight resistance increase for the C3G ceftriaxone and the piperacillin-tazobactam combination (0.047 to 0.094

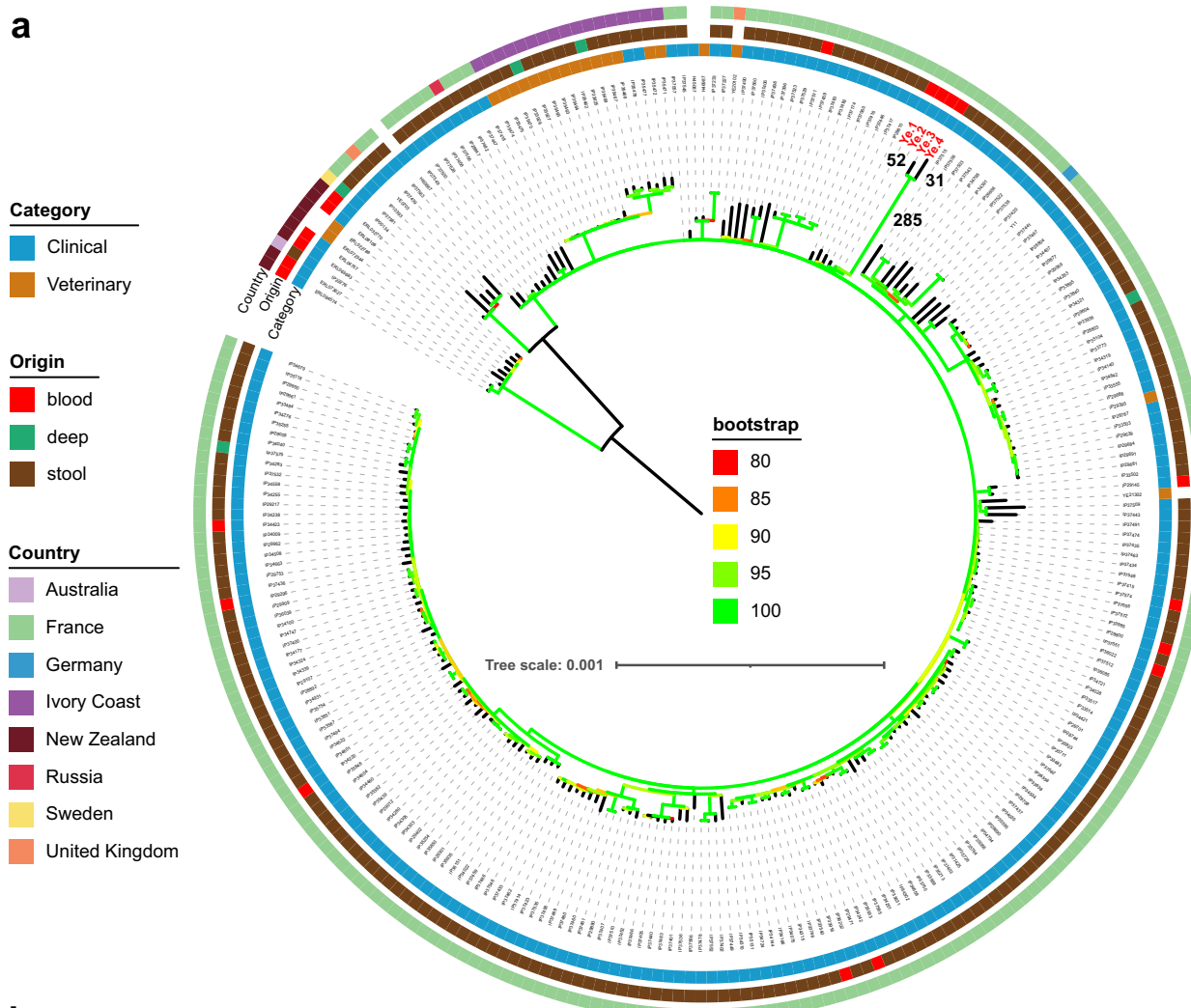


Fig. 3 | Phylogenetic reconstruction. **a** Maximum likelihood phylogeny reconstructed with IQ-TREE2 under TIMEe+ASC model as defined by “ModelFinder” with 100 bootstraps based on 4,738 SNPs identified in 262 strains. The genome of the Y11 strain (NC_017564) was used as reference for variant calling. Numbers close to the branches indicate SNPs numbers. The tree was rooted at midpoint. Branches

are colored according to bootstrap values. Metadata (category, origin, and country) are plotted on 3 colored outer rings. **b** Estimation of the date of internal nodes using least-squares dating (<https://lsdating.pasteur.fr>) among the 4 strains isolated from the patient. Green bars represent the standard deviation of the estimated date.

and 0.19 to 0.38 $\mu\text{g}/\text{mL}$ respectively), suggesting that OmpF truncation could play a role but is not sufficient to promote ceftriaxone resistance in Ye.4. OmpF truncation also led to a slight increase in ciprofloxacin resistance (0.006–0.012 $\mu\text{g}/\text{mL}$) and did not have any effect on the other tested antibiotics such as AG (Table 2).

Additionally, we observed that the stringent response (SR) regulator DksA was potentially truncated in the late isolates due to a large deletion (Supplementary Data 4). As DksA was already described to modulate antimicrobial resistance^{17–20}, we introduced the large deletion from Ye.3 comprising *pncB* and *gluQRS* genes and *dksA* truncation

in Ye.1 (Ye.1-*dksA*^{Ye.3}) and verified the clone by WGS (Supplementary Table 1). By testing antimicrobial susceptibility, we could observe that the deletion of this region increased the susceptibility to most β -lactams and AG while it did not impact ceftriaxone susceptibility (Table 2). This could partially explain Ye.3 and Ye.4 increased susceptibility to AG.

Positive selection of the PitA transporter and TesB thioesterase
A positive selection signal was detected in the phosphate transporter PitA (Supplementary Table 2), where a deletion in its

Table 2 | Antibiotic susceptibility profiling of the Ye.1 and IP29610 wild type and mutated strains

Antibiogram										
Class	Subclass	Antibiotic	Ye.1	IP29610	Ye.1- <i>gyrA</i> ^{Ye.3}	Ye.1- <i>ompF</i> ^{Ye.4}	Ye.1- <i>dksA</i> ^{Ye.3}	Ye.1- <i>pitA</i> ^{Ye.3}	Ye.1- <i>tesB</i> ^{IP29610}	IP29610- <i>tesB</i> ^{Ye.1}
β-lactam	penicillin (4 G)	piperacillin-tazobactam ³	-	-	-	-	-	-	-	-
	penicillin (4 G)	piperacillin	-	-	-	-	S	S	-	-
	penicillin (4 G)	ticarcillin	R	R	R	R	R	R	R	R
	penicillin (3 G)	amoxicillin	R	R	R	R	R	R	R	R
	carbapenem	ertapenem	-	-	-	-	-	-	-	-
	penicillin	ticarcillin-clavulanate	-	-	-	-	-	-	-	-
	cephem (3 G)	ceftazidime	-	S	-	-	S	S	-	-
	cephem (2 G)	cefoxitin	-	-	-	r	S	-	-	-
	penicillin (4 G)	temocillin	-	-	-	-	-	-	-	-
	carbapenem	imipenem	-	-	-	-	-	-	-	-
	penicillin (3 G)	amoxicillin-clavulanate	-	-	-	-	S	-	S	-
	cephem (3 G)	cefotaxime	-	-	-	-	S	-	-	-
	cephem (3 G)	ceftazidime-avibactam	-	-	-	-	-	-	-	-
	carbapenem	meropenem	-	-	-	-	-	-	-	-
	monobactam	aztreonam	-	-	-	-	-	-	-	-
	cephem (4 G)	cefepime	-	-	-	-	-	-	-	-
	cephem (3 G)	moxalactam	-	-	-	-	-	-	-	-
	penicillin	mecillinam	-	-	-	-	-	-	-	-
	cephem (5 G)	ceftolozan-tazobactam	-	-	-	-	S	-	-	-
	cephem	cefiderocol	-	-	-	-	-	-	-	-
quinolone	quinolone	nalidixic acid	-	-	R	-	-	-	-	-
	fluoroquinolone	levofloxacin	-	-	r	-	-	-	-	-
	fluoroquinolone	ciprofloxacin ²	-	-	r	-	-	-	-	-
tetracycline		tigecycline	-	-	-	-	-	-	-	-
fosfomycin		fosfomycin	-	-	-	-	-	-	-	-
nitrofuran		nitrofurantoin	-	-	r	-	S	-	-	r
sulfonamide-trimethoprim		sulfamethoxazole-trimethoprim	-	S	-	-	S	-	-	-
amphenicol		chloramphenicol	-	-	r	-	S	-	-	-
polymyxin		colistin	-	-	-	-	-	-	-	-
aminoglycosides		gentamicin	-	-	-	-	S	-	-	-
		amikacin ³	-	-	-	-	S	S	-	-
		tobramycin	-	-	-	-	S	-	-	-
		netilmicin ¹²	-	-	-	-	S	-	-	-
MIC										
Class	Subclass	Antibiotic	Ye.1	IP29610	Ye.1- <i>gyrA</i> ^{Ye.3}	Ye.1- <i>ompF</i> ^{Ye.4}	Ye.1- <i>dksA</i> ^{Ye.3}	Ye.1- <i>pitA</i> ^{Ye.3}	Ye.1- <i>tesB</i> ^{IP29610}	IP29610- <i>tesB</i> ^{Ye.1}
β-lactam	cephem (3 G)	ceftriaxone ¹²³	0.047	0.047	0.047	0.094	0.047	0.047	0.047	0.064
	cephem (2 G)	cefoxitin	6	4	6	24	2	4	4	6
	penicillin (4 G)	piperacillin-tazobactam ³	0.19	0.19	0.25	0.38	0.094	0.25	0.094	0.19
aminoglycosides and aminoglycosides-like		netilmicin ¹²	0.5	0.75	0.75	0.5	0.25	0.5	0.5	1
		amikacin ³	3	3	3	3	1	2	1.5	4
		tobramycin	0.75	0.75	1	0.75	0.38	0.5	0.75	1.5
		gentamicin	0.75	0.5	1	0.75	0.19	0.5	0.5	1
		spectinomycin	16	24	24	24	32	16	24	48
Quinolone	fluoroquinolone	ciprofloxacin ²	0.006	0.003	0.047	0.012	0.003	0.006	0.004	0.006
	fluoroquinolone	levofloxacin	0.023	0.023	0.125	0.023	0.006	0.006	0.012	0.023

¹Administered treatment between Ye.1 and Ye.2 isolation.²Administered treatment between Ye.2 and Ye.3 isolation.³Administered treatment between Ye.3 and Ye.4 isolation.

3 G: 3rd generation. 4 G: 4th generation. 5 G: 5th generation. -: susceptible. s: increased susceptibility compared to wildtype Ye.1. R: resistance. r: increased resistance compared to wildtype Ye.1. Source data are provided as a Source Data file.

C-terminal region was observed only in Ye.3 and Ye.4, affecting two cytoplasmic, one non cytoplasmic and three transmembrane regions (Fig. 4a, b). The *pitA* allele from Ye.1 was replaced with the Ye.3 *pitA* allele, resulting in the Ye.1-*pitA*^{Ye.3} mutant, validated by WGS (Supplementary Table 1). According to the Yersiniomics database²¹, expression of PitA is downregulated at 37 °C and intracellularly, so we assessed bacterial viability upon phagocytosis by macrophages but could not observe any significant differences between strains, irrespective of the inoculum temperature (Supplementary Fig. 5). In contrast, we observed a slight but constant reduction of AG resistance of Ye.1-*pitA*^{Ye.3} compared to the wild type (WT) Ye.1 strain (Table 2), as reported for a *P. aeruginosa* *pitA* mutant²², suggesting that PitA truncation influences the transporter activity.

Another positive selection signal was present in all isolated strains, in the acyl-CoA thioesterase II *TesB*, which regulates levels of acyl-CoAs, free fatty acids, and coenzyme A. In position 280 of this enzyme, a glycine is conserved in diverse eukaryotic and bacterial species²³ while a serine was present in Ye.1 to Ye.4. Position 280 is located next to the active site of *TesB*, consisting of a Q278, D204 and T228 triad, as well as in the vicinity of dimer interface residues V277 and V281 (Fig. 4c). Mutation in E279, forming a trypsin-like catalytic triad together with H58 and S107 has also been shown to influence *TesB* activity²³. *TesB* structure is highly conserved between *Escherichia coli* and *Yersinia* species²⁴. To understand the structural impact of the G280S substitution, we used the crystal structure of *E. coli* *TesB* dimer and the AlphaFold-predicted structure of Ye IP29610 *TesB* dimer (an isolate close to Ye.1, but which does not harbor the G280S

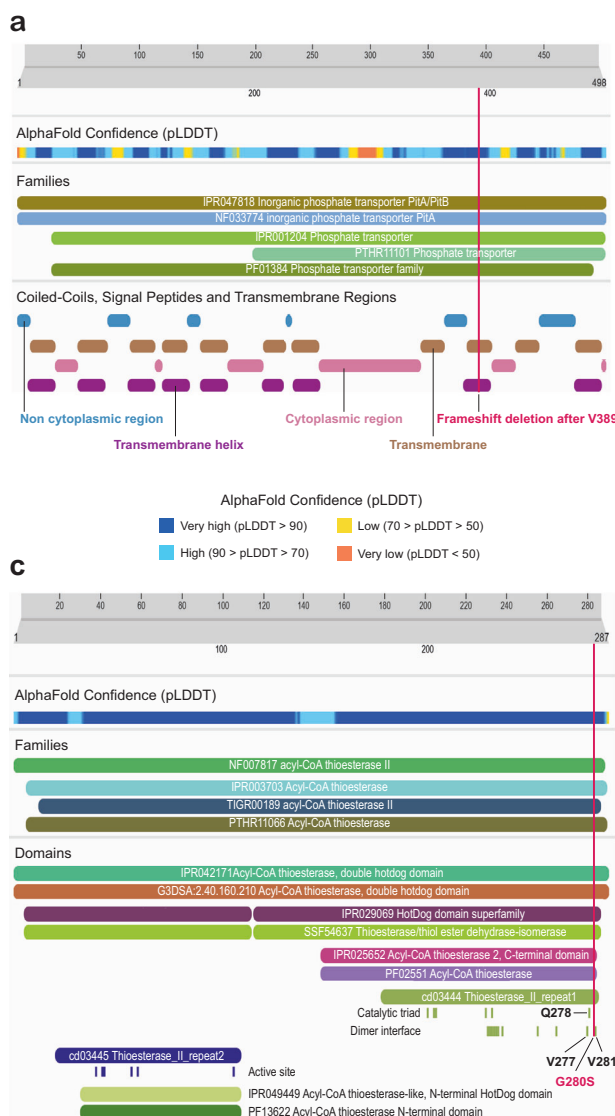
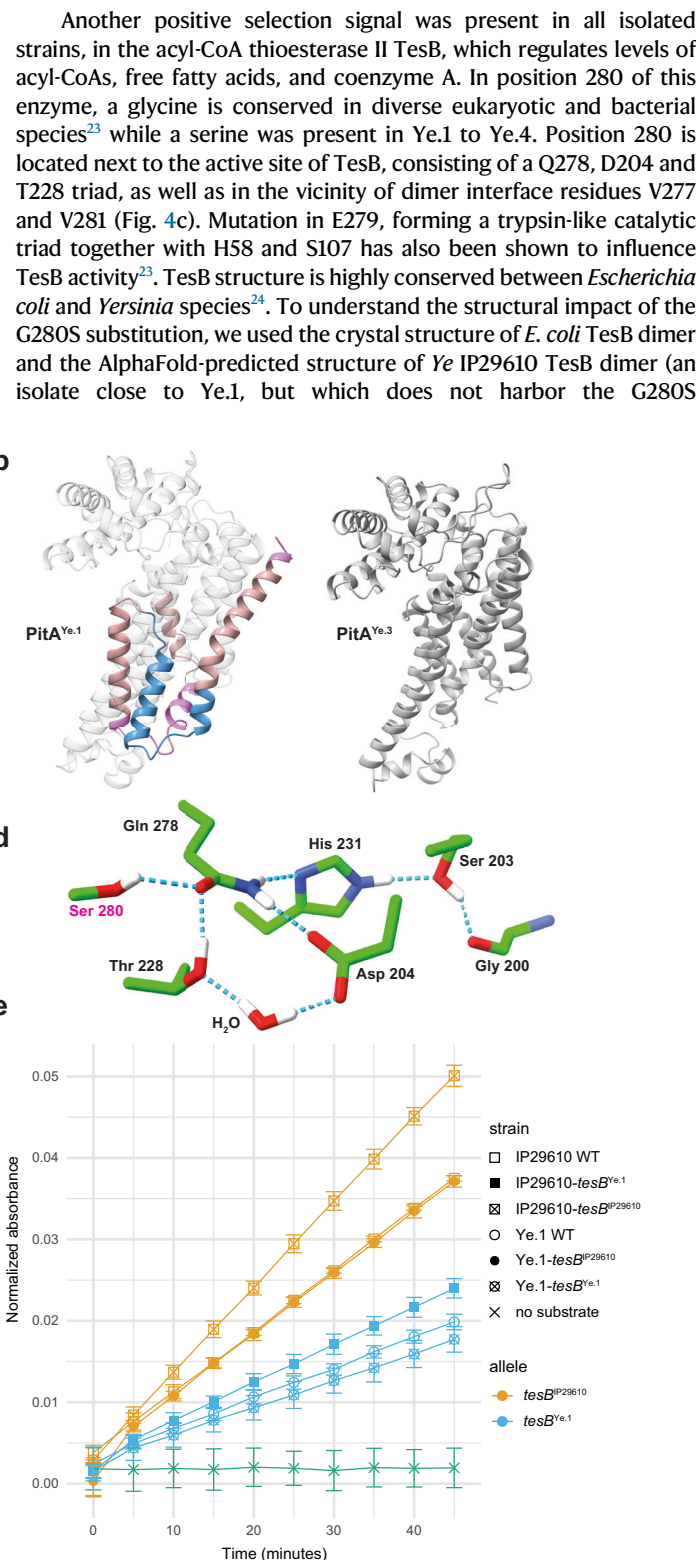


Fig. 4 | Structure and phenotypical analysis of PitA and TesB mutation.

a, c Domain analysis of Y11 PitA and TesB proteins respectively, as found on InterPro on 2025.02.12. Mutation position is shown by a vertical magenta line and residues from the catalytic triad or dimer interface close to the TesB mutation are annotated. Domains are annotated with entry numbers for InterPro (IPR), NCBIfam (NF or TIGR), PANTHER (PTHR) Pfam (PF), CATH-Gene3D (G3DSA), SUPERFAMILY (SSF) or CDD (cd). Non cytoplasmic, cytoplasmic and transmembrane regions are annotated via Phobius and Transmembrane Helix are annotated via TMHMM. AlphaFold confidence (pLDDT) is colored from very low confidence (orange) to very high confidence (dark blue). **b** AlphaFold prediction structure for PitA^{Ye.1} (left) and



PitA^{Ye.3} (right). Truncated residues are displayed with the same color code as the regions in panel (a). **d** Structure of the *TesB* active site of *E. coli* with a G280S mutation, annotated in magenta, showing an additional interfering hydrogen bond from the serine side chain. Carbon atoms are shown in green, oxygen atoms in red, nitrogen atoms in blue and hydrogen atoms in white. **e** Thioesterase II activity of IP29610 and Ye.1 mutant harboring different *tesB* alleles (IP29610 allele in orange and Ye.1 allele in blue), measured by the CoA release from decanoyl-CoA. Each point shows the mean and standard deviation of $n = 3$ replicated wells in one experiment. The green curve represents the negative control without substrate. Source data are provided as a Source Data file.

substitution) (Supplementary Fig. 6a, b). By modeling the G280S substitution in both structure, we observed that the hydroxymethyl side chain of the serine was oriented towards the first catalytic triad (Q278, D204 and T228) but neither toward the dimer interface nor the trypsin-like catalytic triad (Supplementary Fig. 6c, d). We also observed that the hydroxyl group of the S280 side chain could form a hydrogen bond with the oxygen from the Q278 amide group, presumably interfering with the hydrogen bond network, destabilizing the H₂O molecule²³ and impacting the enzymatic activity (Fig. 4d).

To investigate the effect of this mutation on TesB enzymatic activity, we replaced the WT *tesB* gene allele from IP29610 (*tesB*^{IP29610}) with the *tesB* allele from Ye.1-Ye.4 (*tesB*^{Ye.1}), leading to the IP29610-*tesB*^{Ye.1} mutant strain. Similarly, we replaced *tesB*^{Ye.1} by *tesB*^{IP29610} in the Ye.1 genetic background, resulting in the Ye.1-*tesB*^{IP29610} mutant. By assessing thioesterase I and thioesterase II activities of the various WT and mutated strains, we demonstrated that the single amino acid substitution present in the Ye.1 to Ye.4 isolates decreased TesB enzymatic activity (Fig. 4e, Supplementary Fig. 7), while no clear antibiotic susceptibility differences could be observed (Table 2).

Proteome remodeling of *Ye* isolates

To further characterize *Ye* evolution during the course of in-host infection, we analyzed proteomes of the four isolates by mass spectrometry. Out of the ~2,200 proteins identified, 277 proteins were differentially abundant between the two early isolates and 323 proteins between the two late isolates. In contrast, 845 to 1,070 proteins were differentially abundant in the 4 pairwise comparisons of early versus late isolates, which account for almost half of the identified proteome (Supplementary Data 5). These proteome differences correlate with the genetic distances between early and late isolates. The vast majority (85–97%) of the genes coding the differentially abundant proteins in all comparisons belonged to *Ye* core-genome (Supplementary Data 5). Of note, for the remaining accessory genome, the proportion of less abundant proteins was greater in the latest isolates than in the earliest isolate in each comparison. This suggests a global downregulation of the accessory genomes over time during chronic infection.

The annotated proteins from Ye.1 to Ye.4 were mapped to the *Ye* genotype 4 reference strain Y11 (Supplementary Data 6). We validated the 3 large genomic region deletions as well as the impact of the truncations on protein abundance (Supplementary Data 4). Gene set enrichment analysis (GSEA) on biological process gene ontology (GO) terms revealed isolate-specific variations as well as common trends in early versus late isolate comparisons (Fig. 5a). The loss of the pYV virulence plasmid (probably during subculture, a known laboratory artifact) in all strains but Ye.1 could be observed through the enrichment of the type III secretion system term in Ye.1. Ye.2 was specifically characterized by an enriched galactose metabolism proteome. Amino acid biosynthetic process was the most specific enriched term in late isolates versus early isolates. Mapping of the protein abundance comparisons on the global metabolic map of Y11 (Supplementary Fig. 8, 9) and on specific KEGG pathways (Supplementary Data 7) showed a strong metabolic rewiring from early to late isolates, such as a decreased purine, pyrimidine or riboflavin metabolism, one-carbon pool by folate, carbohydrate metabolism and oxidative phosphorylation, and a perturbated amino acid metabolism such as increased histidine, serine, tryptophan or leucine biosynthesis, or reduced arginine or methionine biosynthesis and glycine cleavage (Supplementary Data 7).

Virulence-associated proteins (e.g. attachment locus Ail, fimbriae MyfA, serine protease ecotin, superoxide dismutases or positive regulator RovA) were less abundant in late isolates, while RovM or YmoA negative virulence regulators had an increased abundance (Fig. 5b). Additionally, the invasin Inv was less abundant in Ye.3, and a mutation in its initiation codon (Supplementary Data 2) completely abrogated its production in Ye.4. On the other hand, the chemotactic operon

cheAWYZ was more abundant in late isolates, along increased levels of quorum sensing autoinducer-1 YenI and decreased levels of autoinducer-2 proteins LsrGFBDCARK. While we could not test the differential pathogenicity of the clinical isolates due to loss of the pYV virulence plasmid, we assessed cell invasiveness, which is independent of the type 3 secretion system encoded by pYV genes, with isolates curated from the pYV plasmid. We demonstrated a reduced cell invasion for Ye.4 at 2 h post infection, concordant with Inv inactivation. We additionally observed a reduced ability to replicate inside epithelial cells for the latest isolate compared to early isolates at 6 and 24 h post infection (Supplementary Fig. 10).

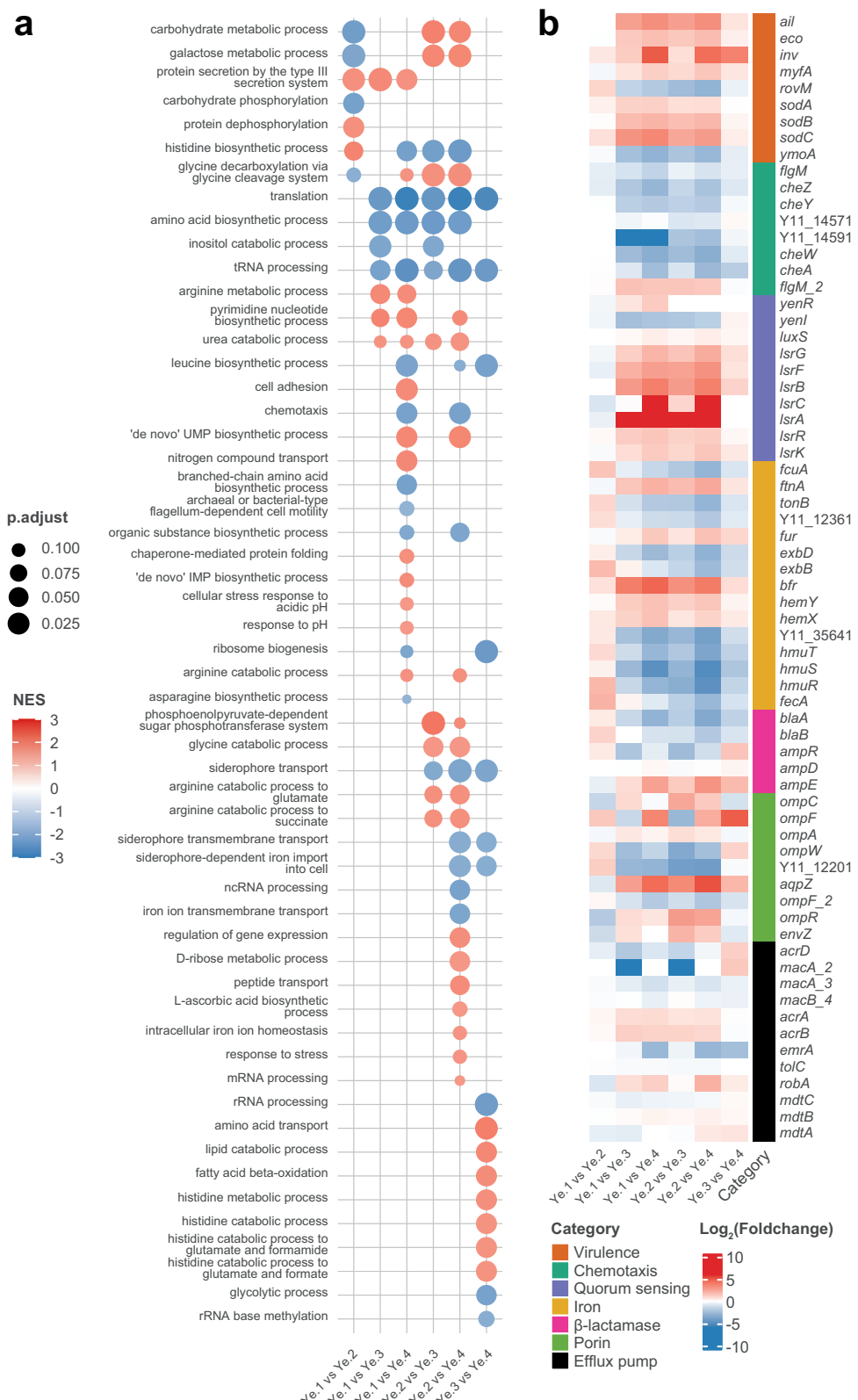
Iron import systems such as the hemin import system encoded by the *hmuRSTUV* operon or the TonB/ExbB/ExbD transport system were more abundant in the late isolates, while iron storage abundance such as the non-heme ferritin FtnA or the bacterioferritin Bfr was decreased (Fig. 5b). These changes correlated with a decreased abundance of the iron metabolism repressor Fur, showing a probable adaptation to the free iron-scarce environment during *Ye* evolution in the bloodstream.

We next analyzed the protein levels of antibiotics resistance and susceptibility factors such as β-lactamases, porins or efflux pumps (Fig. 5b). An increased abundance of the category A β-lactamase BlaA was observed for the late strains and even more in Ye.4, negatively correlating with the regulator AmpE. More importantly, the category C BlaB (or AmpC) β-lactamase was more abundant in the ceftriaxone-resistant isolate Ye.4 compared to all other isolates. In addition to its truncation in Ye.4, the porin OmpF was less abundant in Ye.2 compared to Ye.1, possibly causing a decreased permeability of the outer-membrane to antibiotics. The OmpC porin showed variable abundance levels, correlating with OmpR/EnvZ two components system abundance, while other porins such as OmpW, OmpF_2 and Y11_12201 were much more abundant in the late isolates. Abundance of efflux pump-related proteins did not change significantly, except for the macrolide-specific efflux protein MacA which was only detected in the late isolates and more abundantly in Ye.3, the strain isolated during spiramycin treatment.

Late *Ye* isolates display a perturbed stringent response

To better understand which genetic differences could be the cause of the overall changing proteome, correlation of the 6 pairwise comparisons was measured against 57 published *Ye* transcriptome comparisons that we previously gathered on the Yersiniomics database²¹ (Supplementary Data 8). After clustering by correlation distances, we could define specific biological condition comparisons associated to several clusters, such as temperature switch, culture with or without host cells, or strain comparisons (Fig. 6). Interestingly, one cluster grouped logarithmic versus stationary phase growth comparisons with $\Delta dksA$, $\Delta relA\Delta spoT$ and $\Delta dksA\Delta relA\Delta spoT$ versus WT comparisons²⁵. We defined it as a stringent response-associated cluster (SR cluster), as this mechanism is linked to both *dksA*, *relA* and *spoT* mutants and growth phase transition. Early versus late *Ye* isolate comparisons had a moderate but significant correlation with this cluster, and more specifically with the $\Delta dksA$ versus WT comparison (correlation coefficient: -0.32 to -0.46). Importantly, comparisons of early isolates with Ye.4 had higher correlation coefficients than comparisons of early isolates with Ye.3 when correlating with the SR cluster, which also translated in a significant correlation between Ye.3 versus Ye.4 comparison and the SR cluster. These data suggest that SR is differentially activated in early and late isolates, and even more strongly in Ye.4.

The observation that the “translation” and “tRNA processing” GO terms are upregulated in the late isolates and even more in Ye.4 (Fig. 5a) corroborates the correlations observed with the SR-cluster. Ribosomal- and tRNA-associated proteins were upregulated in both SR mutants²⁵ and late isolates; other accessory molecules and regulators (RimM, RaiA, Hpf), were either down- or up-regulated in a similar manner between SR mutants and Ye.3/Ye.4 (Supplementary Fig. 11).



Other protein abundance changes correlating with SR mutants included increased levels of magnesium/cobalt transporter CorA, sulfur-transferase TusA, the shikimate pathway enzyme AroB and AroK, the porin OmpF_2 or the acetate uptake transporter SatP among others, while some were only depending on *dksA* mutation such as the hemin transporter subunits HmuR, HmuS and HmuT, the proline pathway enzymes ProA and ProB or the porin Y11_12201. On the other hand, SR

mutants were associated with the downregulation of the previously mentioned *lsr* operon, urease *ureABCDEF* and glycogen utilization *glgBXCAP* operons, ferritin Bfr, stress response protein ElaB, superoxide dismutase SodC, entericidin A/B, glycine cleavage system enzyme GcvT and fatty acid degradation enzymes FadA and FadB. SR mutants also correlated with a strong expression decrease of *acs* and *actP*, genes that are truncated in late isolates. Most importantly, the

Fig. 5 | Ye proteomic analysis. **a** Gene set enrichment analysis (GSEA) of biological process gene ontology terms across pairwise comparisons of *Ye* proteomes. Positive normalized enrichment scores (NES) calculated by GSEA algorithm are shown in red and correspond to enriched terms in the first isolate in the comparison, while negative NES are shown in blue and correspond to enriched term in the second isolate in the comparison. The nominal p-value is calculated according to GSEA algorithm. Multiple testing is adjusted by the Benjamini-Hochberg procedure (p.adjust). **b** Heatmap for all pairwise comparisons of protein differential

abundance between the 4 clinical isolates, with the corresponding genes displayed on the right. Proteins are grouped in categories with different colors based on Y11 RefSeq and Uniprot annotations, and bibliography. $\log_2(\text{foldchange})$ shown in red corresponds to a protein more abundant in the first isolate in the comparison, while $\log_2(\text{foldchange})$ shown in blue corresponds to a protein more abundant in the second isolate in the comparison. In each category, proteins are ordered by Y11 locus order. Source data are provided as a Source Data file.

stationary phase sigma factor RpoS (σ^S) and growth-dependent metabolism regulator Fis were down- and upregulated, respectively, in both SR mutants and late isolates, which could contribute to the differential abundance of ribosomal and metabolic enzymes. These results highlight the pivotal role of SR in metabolism regulation and its probable implication during in-host evolution under antibiotics exposure.

Discussion

This study documents a previously undescribed chronic *Ye* infection case due to a strain evolving in the same patient. Between December 1999 and October 2013, antibiotics were apparently successful in the treatment of five independent *Ye* bacteremia episodes; however, discontinuation of antibiotics was always followed by a new bacteremia. The appearance of vegetations observed by echocardiography in 2006, and their disappearance during therapy, argue for *Ye* growth on the atrial lead of the pacemaker and release into the bloodstream during the antibiotic discontinuation periods.

Genomic and proteomic analyses of four *Ye* strains (Ye.1 to Ye.4) isolated from the patient allowed us to identify different mechanisms of resistance to various antibiotic classes. Resistance to nalidixic acid was already observed from August 2001 after long-term ciprofloxacin treatment. Resistance to quinolones usually involves mutations in the QRDR of the *gyrA* gene, leading either to (i) a change of glycine 81 into cysteine, (ii) a change of serine 83 into arginine, isoleucine, or cysteine, or (ii) a change of aspartic acid 87 into a tyrosine, asparagine, or glycine^{13,14,26,27}. In Ye.3 and Ye.4, we observed a previously undescribed deletion of 3 nucleotides in the *gyrA* QRDR, leading to substitution of aspartic acid 82 and serine 83 by a unique glycine. Our work thus identifies a previously undescribed mutation in *gyrA* leading to quinolone resistance.

After the long-term ciprofloxacin treatment was changed to C3G ceftriaxone, Ye.4 became resistant to cefoxitin and ceftriaxone. Abrogation of OmpF porin production is a widely shared strategy to reduce membrane permeability to antibiotics and was shown to be induced in *E. coli* upon exposure to ceftriaxone¹⁵. A study showing OmpF (YOMP-C in this previous work) mutations selected by cefoxitin treatment in *Ye* and leading to increased β -lactam resistance supports the antibiotic import via this porin¹⁶. β -lactamase induction has long been studied in *Ye*²⁸ and a recent study suggested an increased BlaB inducibility in *Ye* biotypes 2 and 4²⁹. According to our present work, while OmpF truncation alone was not sufficient to induce ceftriaxone resistance in Ye.1, the class A β -lactamase BlaA and class C β -lactamase BlaB (or AmpC) were more abundant in the Ye.4 isolate, probably playing a synergistic role together with the porin inactivation, as both β -lactamases have been shown to be involved in ceftriaxone resistance in *Ye* biotype 1B³⁰. Interestingly, the macrolide efflux pump MacA was more expressed in Ye.3, which was isolated during the pneumonia treatment with the macrolide spiramycin.

The SR regulator DksA was also brought to light as a key element modulating antimicrobial susceptibility, with variable results depending on the pathogens, strains or experimental conditions^{17–20}. Interestingly, in our case, insertion of the region corresponding to the deletion, i.e. comprising *pncB*, *gluQRS* genes and *dksA* truncation,

in Ye.1 led to increased susceptibility to AG, to nearly all β -lactams except ceftriaxone (used as a long-term treatment), as well as to other antibiotic classes, confirming and expanding previous results on *Ye*¹⁷. Additionally, we observed that the *pitA* truncation could also contribute to the AG susceptibility²², and a *rlmE* (or *rrmJ/ftsJ*) mutation, found in the late isolates, could also lead to an increased susceptibility to chloramphenicol, gentamicin, spectinomycin and other antibiotics as shown in *E. coli*³¹. The role of other mutated genes, such as *mfd*, previously shown to be involved in antibiotics resistance evolvability³² remains to be further investigated in the context of in-host evolution.

We observed an increased ciprofloxacin MIC of late isolates when assaying by microdilution in LB, which is a complex and non-standardized medium unsuitable for MIC assessment, but necessary for our survival experiments. Nevertheless, exposure to ciprofloxacin concentrations higher than the MIC showed an increased tolerance of Ye.3, which could be explained by the severe growth defect observed for Ye.X (which was isolated after ciprofloxacin treatment), Ye.3 and Ye.4^{6,33}. In the late isolates, we identified mutations in genes involved in metabolism or growth. The cumulative mutations in genes encoding the RNA polymerase subunits RpoC³⁴ and RpoD, the DNA topoisomerase ParE³⁵, the 50S ribosomal protein RplF³⁶, the rRNA methyltransferase RlmE/RrmJ/FtsJ^{31,37} or the SR regulator DksA^{17,18,38} could account for slow growth. Proteomics analysis of the isolates revealed a strong metabolic rewiring with reduced carbohydrate utilization and reduced purine, pyrimidine, riboflavin and folate metabolisms, together with decreased respiration, which overall corroborate the slow growth phenotype.

Vegetations detected on the pacemaker argue for the formation of a biofilm by the *Ye* strains. *Ye* biofilm production has been reported on medical devices such as feeding tubes³⁹ and can account for antibiotic treatment failure^{6,40}. We identified several mutations in Ye.3 and Ye.4 which can be associated with loss of motility and planktonic growth, favoring biofilm formation: for example, mutation of the flagellar genes *flgD* in both Ye.3 and Ye.4, and *flgG* and *flgA* in Ye.4. In this direction, no flagellar proteins were detected for any isolate in our culture conditions, in agreement with the reported low flagellar expression in *Yersinia* species at 37 °C⁴¹. Additionally, a decreased expression or inactivation of adherence and invasion factors to host cells such as Ail, MyfA or Inv could favor adhesion to an abiotic surface by other adhesins. However, proteomics observations regarding higher levels of chemotaxis and quorum sensing AI-1 as well as lower levels of quorum sensing AI-2 protein in late isolates prevent us to draw definitive conclusions on biofilm formation capacities of these isolates. A recent study of SR in *Ye* also showed complex interactions between SR genes and biofilm forming capability, preventing any further interpretation¹⁷.

In addition to the evolutive pressure of antibiotics, *Ye* faced the host immune system, nutritional immunity as well as a specific environment requiring a metabolic switch to adapt to a new lifestyle in the blood⁴². Requirements of amino acids such as tryptophan for survival in blood could explain the perturbed amino acid biosynthesis pathways in late isolates. Recent studies also highlighted the role of glycine and other amino acids in complement susceptibility, pointing to metabolism adaptation as

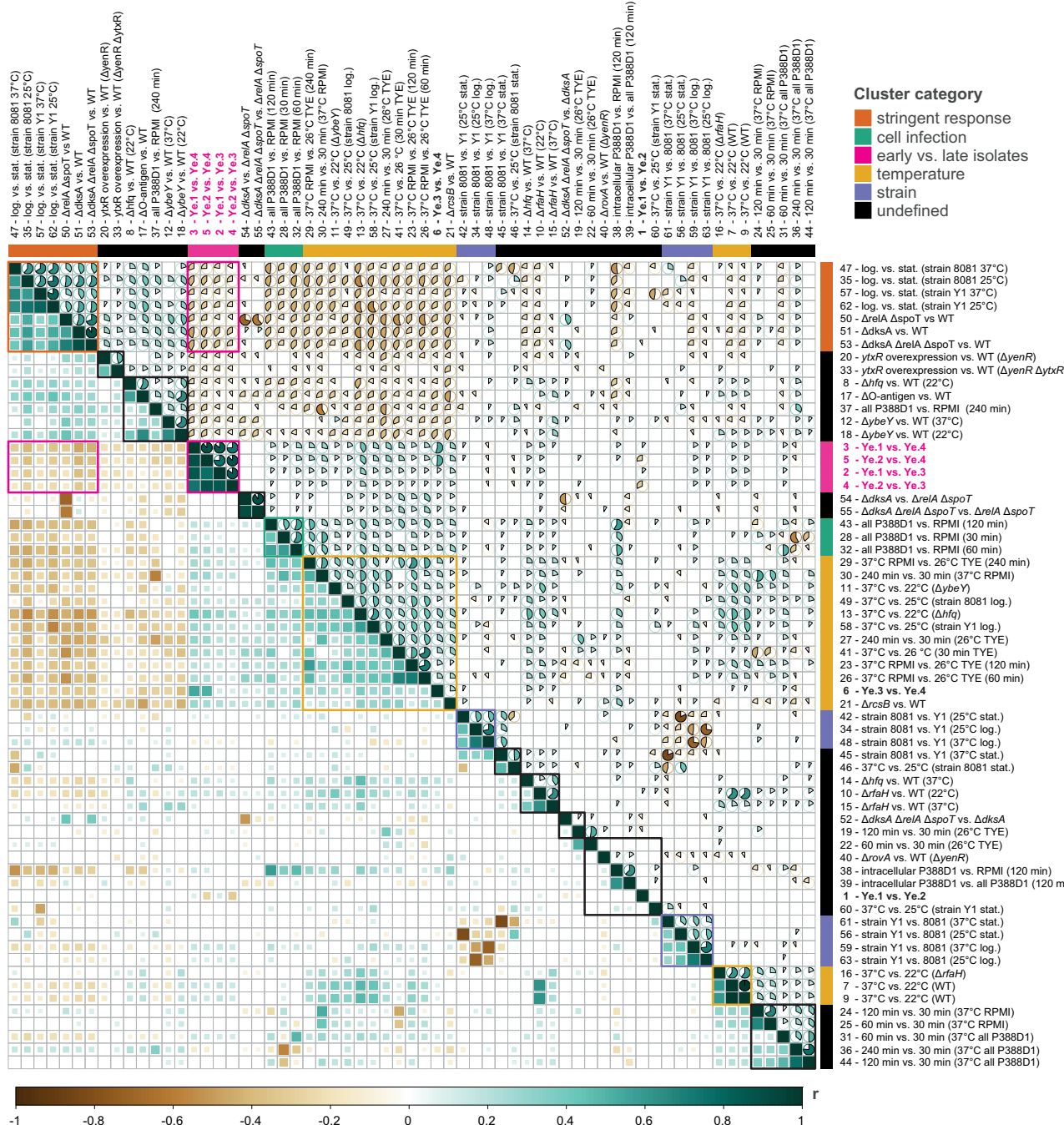


Fig. 6 | Heatmap of omics comparison correlations. Spearman correlation of 63 Ye omic experiment comparisons, clustered by hierarchical clustering and showing 15 clusters (squares). Color code of manually annotated clusters is shown on the top and right of the heatmap, and cluster squares are colored accordingly. Ye.1-Ye.4 isolate proteome comparisons are in bold, with early versus late isolate comparisons colored in magenta and their correlations with the stringent response cluster highlighted by two magenta rectangles. Upper part of the heatmap is a pie

representation (the correlation coefficient is represented by color and filling of the pie) and lower part is a square representation (the correlation coefficient is represented by color and size of the square). Only correlation coefficient with a p-value < 0.001 are shown. Coefficient (r) color scale is shown at the bottom. log.: logarithmic phase. stat.: stationary phase. vs.: versus. Source data are provided as a Source Data file.

a way to better survive complement^{43,44}. Free iron scarcity in blood favored upregulation of iron uptake and reduced abundance of iron storage proteins. Interestingly, loss of the pore-forming toxin YaxAB (*Y1_10331/Y1_10321*) as well as reduced abundance of virulence factors such as Ail, MyfA, superoxide dismutases, ecotin, invasin or the regulator RovA suggest that bacteria defective for pathogenic functions that carry a fitness cost can be selected to favor host adaptation^{1,45-47}.

In our late isolates which show a perturbed SR, purine biosynthesis was strongly downregulated, and the pppGpp pyrophosphatase GppA (or Ppx) and the SR regulator DksA were mutated, probably reinforcing unbalanced (p)ppGpp levels. Additionally, the Ye.4 isolate showed an even closer proteome to SR mutants than Ye.3, as shown by the higher ribosomal content or decreased fatty acid degradation pathway for example^{25,38}, suggesting that ceftriaxone-resistant Ye.4 possesses a more dysregulated stringent

response than Ye.3. This could be due to Ye.4-specific OmpF inactivation, reducing nutrient import, however we cannot formally exclude that other SNPs present in Ye.3 or Ye.4 genes are also involved in the observed phenotype. Whether adaptation to the host environment⁴⁸ played a more important role than the antibiotic treatment⁴⁹ in selecting the perturbed SR in the late isolates remains to be deciphered; nevertheless, it is interesting to mention that a GppA truncation was recently shown to be a crucial step in *Y. pestis* evolution toward human host adaptation⁵⁰.

Positive selection analysis revealed two proteins whose activity was changed during in-host evolution. TesB thioesterase was mutated in all *Ye* clinical isolates which showed reduced enzymatic activity. The first strain was isolated before any known antibiotic treatment, and TesB mutants showed no clear changes in antibiotic susceptibility profiles, suggesting that the mutation was selected for host adaptation rather than antibiotics tolerance and resistance. *Ye* thioesterase II activity was impacted by the TesB mutation, while thioesterase I activity was not, suggesting that this latter is accomplished by another enzyme such as TesA. Interestingly, TesA and YciA thioesterases were more abundant in late than early isolates, confirming the importance of thioesterase activity during in-host evolution. TesA is specific for long-chain acyl-CoA ester, while TesB has a broader substrate range⁵¹, highlighting a fine-tuning of carbon utilization according to fatty-acid availability in blood. On the other hand, PitA truncation was only observed in late isolates and probably led to loss of function. PitA is downregulated at 37 °C, suggesting a role in the environment outside of the mammalian host²¹. Whether this mutation was observed because of a specific selection pressure or because of the absence of counter-selection in the host remains to be deciphered.

Omics analyses showed a reduction in genome size during in-host evolution, as described in other species², as well as a downregulation of non-core genome genes. Additionally, the relatively high evolutionary rates observed were in the expected range of short term in-host evolution, possibly due to strong genetic bottlenecks and lack of purifying selection¹. However, branches leading to the late isolates showed 60–80% lower inferred evolutionary rates compared to those leading to the early isolates, probably reflecting the slower growth rates of the later isolates, mimicking results observed for persister strains of Ebola virus⁵² or *Mycobacterium tuberculosis*⁵³.

In conclusion, we report the unusual clinical case of a patient with iterative bacteremia and endocarditis due to a *Ye* bioserotype 4/O:3 strain evolving over a period of 14 years. The last two isolates, which were simultaneously evolving in the patient, accumulated mutations that allowed antibiotic resistance, including a previously unknown substitution conferring resistance to quinolones, and antibiotic tolerance. The latter phenotype was associated with a reduction in genome size and loss of essential functions for growth in vitro, while retaining the ability to survive in the host. The last isolated strains caused bacteremia despite the continuity of the antibiotic treatment, highlighting the transition occurring between early onset tolerance and resistance, a critical problem in antibiotic treatment that should urgently be addressed⁵. Our findings have implications in case management, as they reinforce the need for early pacemaker removal in addition to antibiotic therapy⁵⁴. They may also guide future design of more effective treatments for chronic and biofilm-associated bacterial infections. If the infected material cannot be removed as it was the case in our study, the choice of the right antibiotic is crucial. It must be well tolerated by the patient, be active on the biofilm and should not promote the emergence of resistance nor tolerance. It appears here that long-term ceftriaxone has been well tolerated, however it probably induced tolerance and resistance to this antibiotic. A better understanding of mechanisms modulating antibiotic tolerance will be instrumental for optimal treatment of long-term infections.

Methods

Our research complies with the relevant ethical regulations and has been approved by the Ethics Committee In Human Research of the Tours Hospital (France) under the project number 2025 032.

Phenotypic characterization

Bacterial strains were identified using the VITEK2 GN card (bioMérieux) and were sent to the *Yersinia* National Reference Laboratory (Institut Pasteur) for species confirmation/characterization as described⁵⁵. For the growth curves, bacteria were precultured in 5 mL lysogeny broth (LB) at 37 °C under agitation at 200 rotation per minute (rpm) for 16 to 96 h. Precultures were adjusted to OD_{600nm} = 1, and 2.5 mL were inoculated in 250 mL LB. Incubations were performed either at 28 °C or 37 °C under agitation at 200 rpm. Optical density at 600 nm was recorded at different time points to monitor growth of the isolates. Mid-exponential phase growth rate was calculated between 2 and 4 h for Ye.1 and Ye.2, and between 7 and 31 h for Ye.3 and Ye.4.

Antibiotic resistance and tolerance assays

The antibiotic resistance profiles of the bacterial strains were first determined using VITEK2 (bioMérieux) and by disk diffusion method on Mueller-Hinton agar supplemented with 5% horse blood (bioMérieux) for growth deficient isolates during the course of the clinical case. A more comprehensive antibiotic resistance profiling and minimal inhibitory concentration (MIC) measurement was respectively performed by disk diffusion method and Etest on Mueller-Hinton agar supplemented with 5% horse blood (bioMérieux) for the four strains kept in collection at the end of the clinical case. Antibiotic resistance profiling and MIC measurement for the constructed mutants were performed on Mueller-Hinton agar. Interpretation was performed according to the recommendations of the Antibiogram Committee of the French Society for Microbiology. For microdilution and tolerance assays, the four isolates were grown in 4.5 mL LB at 37 °C to reach an optical density (OD_{600nm}) between 0.1 and 1, equivalent to around 10⁸ and 10⁹ bacteria per mL respectively. Microdilution assays were performed by seeding 5.10⁵ bacteria in 100 µL LB in 96-well plates with increasing concentration of antibiotics and incubated for 48 h at 37°C. Survival curves were done by seeding 10⁶ bacteria in 500 µL LB with antibiotics in deepwell plates and incubated at 37°C with an agitation of 180 rpm, with 20 µL periodic sampling for live bacterial enumeration.

Whole genome sequencing and analysis

Bacterial genomes were sequenced and whole genome-based taxonomic assignment was obtained using a 500-gene cgMLST-*Yersinia* as previously described⁵⁶ (see Supplementary methods). 229 epidemiologically unrelated *Ye* 4/O:3 strains isolated in France between 1982 and 2016 were randomly selected and their genome sequenced and public genomes of 34 additional strains were used for subsequent analysis (Supplementary Data 1). The isolation dates of the selected French strains encompass those of Ye.1 to Ye.4, thereby reflecting the diversity of strains circulating in France during this period. Genomes assemblies' statistics of the 263 isolates (Ye.1 to Ye.4) were determined using CheckM version 1.1.3 (Supplementary Data 9). Paired-end FASTQ files were used for variant calling using the Y11 reference strain (accession number: NC_017564) with Snippy version 4.1.0⁵⁷. SNP and small insertions/deletions (up to 50 bp) were identified with snippy with a minimum coverage of 10X, and allele frequency > 0.9, regardless of their annotation (genes or intergenic regions). Putative recombinogenic regions were detected and masked with Gubbins version 2.3.4⁵⁸. A maximum-likelihood phylogenetic tree was built from an alignment of 4,738 chromosomal SNPs with IQ-TREE2 version 2.0.6⁵⁹. Tree visualization was created with iTOL v6⁶⁰. The Least-squares dating tool (<https://lsdating.pasteur.fr>) was used to estimate dates from phylogeny.

Pan-genome phylogenetic analysis

A total of 96 *Ye* strains were randomly selected from the 263 genomes used in this study along with the *Ye*.1-4 for Phylogenetic Analysis by Maximum Likelihood (PAML v1.3.1)⁶¹; the number of strains was chosen to ensure a reasonable computational time. A pan-genome was constructed using PPanGGOLiN v1.1.72⁶² with 80% coverage and 80% amino acid sequence's identity for gene clustering. Each gene of the pan-genome (5,532 genes) was translated to proteins and aligned using MAFFT v7.407⁶³, allowing to search for genes specific to *Ye* isolates. A strict core-genome (100%) of the four *Ye* isolates was identified and consists in 3,829 genes. Back translation to nucleotide was performed to obtain codon alignment, and a phylogenetic tree was built for each gene using IQ-TREE v1.6.7.2⁶⁴. IQ-TREE's ModelFinder⁶⁵ was used to estimate the best variant of the General Time Reversible (GTR) model. The 3,612 genes for which the strains *Ye*.3 and *Ye*.4 are not sisters in the tree were removed. Synapomorphies were analyzed using a dedicated script (<https://gitlab.pasteur.fr/GIPhy/findSynapomorphies/>). PAML tests detected genes under positive selection pressure.

Mutagenesis

Allelic exchanges between the various *Ye* strains were performed by double crossover using the pKNG101 suicide plasmid⁶⁶. We first verified that the 1,000 base pairs upstream and downstream of the target mutation were 100% identical between the template strain (harboring the target mutation) and the recipient strain. We amplified this fragment by polymerase chain reaction (PCR) in the template strain and cloned it in pKNG101 plasmid by Gibson assembly. One ShotTM PIR2 chemically competent *E. coli* were transformed with the resulting plasmid. Successful transformations were selected on LB agar plates supplemented with 50 µg/mL streptomycin and presence of the insert was screened by PCR. We verified the constructed plasmid by Nanopore sequencing and *E. coli* SM10 were transformed with the validated plasmid. We then conjugated the SM10 harboring the construct with the recipient *Ye* strain, in presence of *E. coli* HB101 harboring the pRK2013 helper plasmid. We selected the *Ye* merodiploid strains on LB agar plates supplemented with 100 µg/mL streptomycin and 50 µg/mL carbenicillin, to which our *Ye* clinical isolates were naturally resistant. We screened by PCR both WT and mutant alleles in the merodiploid strains, which were then grown in LB at 28 °C and plated on LB without NaCl + 10% sucrose to select for absence of the pKNG101 *sacB* gene. For the *gyrA* mutations, we performed a disk diffusion assay using a nalidixic acid disk to select resistant clones in the inhibition area. Clones were screened for the presence of the target mutation and absence of the WT allele, and we kept both mutated clones harboring the target mutation, and the "reverted" clones that harbored the WT allele. Some mutants were validated by WGS. PCR primers and programs are listed in Supplementary Data 10.

Structure modelisation and prediction

E. coli TesB structure was downloaded on RCSB-PDB (1C8U) and loaded on ChimeraX 1.9. G280S substitution was generated with the rotamers tool (dynamomics library) and the rotamer minimizing the number of clashes was chosen. Hydrogen-bond were modeled with the default parameter. *Ye* TesB dimer and PitA monomer structures were predicted using AlphaFold server (on 2025 February 21th) and edited with ChimeraX 1.9.

Thioesterase activity

Thioesterase activity was measured as described before⁶⁷. Bacteria were grown at 28°C (if not stated otherwise) in LB overnight. The 5 mL overnight cultures were centrifuged at 5,000 x g for 20 min at room temperature. The bacterial pellets were lysed and assessed for thioesterase activity (see Supplementary methods).

Mass spectrometry-based proteomics

Ye.1 and *Ye*.2 strains were grown overnight in LB at 37 °C under agitation at 200 rpm. 200 µL of the culture were plated on 5 tryptic soy agar (TSA) plates and incubated for 24 h at 37 °C. *Ye*.3 and *Ye*.4 were grown for 3 days in LB at 37 °C under agitation at 200 rpm, then 200 µL of the culture were plated on 5 TSA plates and incubated for 48 h at 37 °C. For all *Ye* strains, the bacteria were resuspended with an inoculation loop from the TSA plates in 1 mL phosphate buffered saline (PBS) and washed two times by centrifugation and resuspension in PBS. Bacterial pellets were randomized, then lysed for protein extraction and digestion before analysis by liquid chromatography and tandem mass spectrometry (LC-MS/MS) as explained in Supplementary methods. For the 4 *Ye* strains, 5 biological replicates were processed for a total number of 20 samples.

Proteome analysis

Annotated proteins of *Ye*.1 to *Ye*.4 strains were blasted on the *Y11* reference proteome (RefSeq annotation from December 2022, accession GCF_000253175.1), and the best hit for each *Y11* protein was kept. For each pairwise comparison based on the *Ye*.1 to *Ye*.4 loci database described in the Supplementary methods, the duplicated *Y11* loci were removed by keeping the less differentially expressed value, assuming the duplicated loci came from an annotation of a protein carrying a SNP. The R package clusterProfiler v4.6.2 was used for enrichment and gene set enrichment analysis⁶⁸. The GSEA function was used based on the *Y11* loci by mapping to an in-house annotation file extracted from the *Y11* Gene Ontology terms downloaded from the QuickGo website accessed on May 25th 2023⁶⁹. Analysis was performed on proteins detected in both conditions of each comparison, with all the proteins identified in the experiments as statistical background. Published transcriptomes were downloaded from the Yersiniomics website²¹. *Ye* 8081, *Y1* and *Y11* reference genomes were blasted to find homologous loci, and proteomes and transcriptomes were fused in a unique data-frame. Spearman correlations and p-values of the foldchanges were calculated in R with the Hmisc v5.2.2 package, clustered and displayed by hierarchical clustering with the ward.D2 method using the corplot v0.95 package.

Reporting summary

Further information on research design is available in the Nature Portfolio Reporting Summary linked to this article.

Data availability

Source data are provided with this paper. The genomic data generated in this study have been deposited in the European Nucleotide Archive database under accession code PRJEB19854. Sample ID starting with ERS and accession numbers starting with FWC: *Ye*.1 (ERS1580350, FWCF02000001-FWCF02000181), *Ye*.2 (ERS1580351, FWCE02000001-FWCE02000227), *Ye*.3 (ERS1580352, FWCB02000001-FWCB02000195), and *Ye*.4 (ERS1580353, FWCD02000001-FWCD02000173). <https://www.ebi.ac.uk/ena/browser/view/PRJEB19854>. The mass spectrometry proteomics data generated in this study have been deposited in the ProteomeXchange Consortium via the PRIDE partner repository⁷⁰ under accession code PXD043567. <https://proteomecentral.proteomexchange.org/cgi/GetDataset?ID=PXD043567>. Source data are provided with this paper.

Code availability

R scripts were deposited on Zenodo⁷¹.

References

1. Didelot, X., Walker, A. S., Petro, T. E., Crook, D. W. & Wilson, D. J. Within-host evolution of bacterial pathogens. *Nat. Rev. Microbiol.* **14**, 150–162 (2016).

2. Grote, A. & Earl, A. M. Within-host evolution of bacterial pathogens during persistent infection of humans. *Curr. Opin. Microbiol.* **70**, 102197 (2022).
3. Dekker, J. P. Within-host evolution of bacterial pathogens in acute and chronic infection. *Annu Rev. Pathol.* **19**, 203–226 (2024).
4. Shepherd, M. J. et al. Ecological and evolutionary mechanisms driving within-patient emergence of antimicrobial resistance. *Nat. Rev. Microbiol.* **22**, 650–665 (2024).
5. Levin-Reisman, I. et al. Antibiotic tolerance facilitates the evolution of resistance. *Science* **355**, 826–830 (2017).
6. Dengler Haunreiter, V. et al. In-host evolution of *Staphylococcus epidermidis* in a pacemaker-associated endocarditis resulting in increased antibiotic tolerance. *Nat. Commun.* **10**, 1149 (2019).
7. Miller, C. R., Monk, J. M., Szubin, R. & Berti, A. D. Rapid resistance development to three antistaphylococcal therapies in antibiotic-tolerant *Staphylococcus aureus* bacteremia. *PLoS One* **16**, e0258592 (2021).
8. Elgrail, M. M. et al. Convergent evolution of antibiotic tolerance in patients with persistent methicillin-resistant *Staphylococcus aureus* bacteremia. *Infect. Immun.* **90**, e0000122 (2022).
9. Carniel, E. et al. *Y. enterocolitica* and *Y. pseudotuberculosis*. in *The Prokaryotes* (ed. Springer) vol. 6 270–398 (Dworkin, New York, 2006).
10. The European Union One Health 2022 Zoonoses Report. *EFSA Journal* **21**, (2023).
11. Bottone, E. J. *Yersinia enterocolitica*: the charisma continues. *Clin. Microbiol. Rev.* **10**, 257–276 (1997).
12. Hoogkamp-Korstanje, J. A. A., de Koning, J. & Heesemann, J. Persistence of *Yersinia enterocolitica* in man. *Infection* **16**, 81–85 (1988).
13. Capilla, S. et al. Characterization of the molecular mechanisms of quinolone resistance in *Yersinia enterocolitica* O:3 clinical isolates. *J. Antimicrob. Chemother.* **53**, 1068–1071 (2004).
14. Sihvonen, L. M. et al. Multilocus variable-number tandem-repeat analysis, pulsed-field gel electrophoresis, and antimicrobial susceptibility patterns in discrimination of sporadic and outbreak-related strains of *Yersinia enterocolitica*. *BMC Microbiol.* **11**, 42 (2011).
15. Ching, C. & Zaman, M. H. Identification of multiple low-level resistance determinants and coselection of motility impairment upon sub-MIC ceftriaxone exposure in *Escherichia coli*. *mSphere* **6**, e0077821 (2021).
16. Brzostek, K. & Hrebenda, J. Outer-membrane permeability to β -lactam antibiotics in *Yersinia enterocolitica*. *J. Gen. Microbiol.* **134**, 1535–1540 (1988).
17. Huang, C., Meng, J., Li, W. & Chen, J. Similar and divergent roles of stringent regulator (p)ppGpp and DksA on pleiotropic phenotype of *Yersinia enterocolitica*. *Microbiol. Spectr.* **10**, e0205522 (2022).
18. Willcocks, S. et al. Genome-wide assessment of antimicrobial tolerance in *Yersinia pseudotuberculosis* under ciprofloxacin stress. *Microbiol. Spectr.* **5**, e000304 (2019).
19. Viducic, D. et al. Functional analysis of *spoT*, *relA* and *dksA* genes on quinolone tolerance in *Pseudomonas aeruginosa* under nongrowing condition. *Microbiol. Immunol.* **50**, 349–357 (2006).
20. Maharjan, R. P. et al. DksA is a conserved master regulator of stress response in *Acinetobacter baumannii*. *Nucleic Acids Res.* **51**, 6101–6119 (2023).
21. Lê-Bury, P. et al. Yersiniomics, a multi-omics interactive database for *Yersinia* species. *Microbiol. Spectr.* **11**, e0382622 (2023).
22. Zhao, X. et al. *Pseudomonas aeruginosa* phosphate transporter PitA (PA4292) controls susceptibility to aminoglycoside antibiotics by regulating the proton motive force. *Antimicrob Agents Chemother.* **66**, (2022).
23. Li, J., Derewenda, U., Dauter, Z., Smith, S. & Derewenda, Z. S. Crystal structure of the *Escherichia coli* thioesterase II, a homolog of the human Nef binding enzyme. *Nat. Struct. Biol.* **7**, 555–559 (2000).
24. Swarbrick, C. M. D., Perugini, M. A., Cowieson, N. & Forwood, J. K. Structural and functional characterization of TesB from *Yersinia pestis* reveals a unique octameric arrangement of hotdog domains. *Acta Crystallogr. D. Biol. Crystallogr.* **71**, 986–995 (2015).
25. Huang, C., Li, W. & Chen, J. Transcriptomic analysis reveals key Roles of (p)ppGpp and DksA in regulating metabolism and chemotaxis in *Yersinia enterocolitica*. *Int. J. Mol. Sci.* **24**, 7612 (2023).
26. Drummond, N., Stephan, R., Haughton, P., Murphy, B. P. & Fanning, S. Further characterization of three *Yersinia enterocolitica* strains with a nalidixic acid-resistant phenotype isolated from humans with diarrhea. *Foodborne Pathog. Dis.* **10**, 744–746 (2013).
27. Sanchez-Cespedes, J. et al. Clonal dissemination of *Yersinia enterocolitica* strains with various susceptibilities to nalidixic acid. *J. Clin. Microbiol.* **41**, 1769–1771 (2003).
28. Pham, J. N., Bell, S. M., Martin, L. & Carniel, E. The beta-lactamases and beta-lactam antibiotic susceptibility of *Yersinia enterocolitica*. *J. Antimicrob. Chemother.* **46**, 951–957 (2000).
29. Singhal, N., Pandey, D., Singh, N. S., Kumar, M. & Virdi, J. S. Exploring the genetic determinants underlying the differential production of an inducible chromosomal cephalosporinase - BlaB in *Yersinia enterocolitica* biotypes 1A, 1B, 2 and 4. *Sci. Rep.* **10**, 10167 (2020).
30. Bent, Z. W. & Young, G. M. Contribution of BlaA and BlaB β -lactamases to antibiotic susceptibility of *Yersinia enterocolitica* biovar 1B. *Antimicrob. Agents Chemother.* **54**, 4000 (2010).
31. Caldas, T., Binet, E., Bouloc, P. & Richarme, G. Translational defects of *Escherichia coli* mutants deficient in the Um2552 23S ribosomal RNA methyltransferase RrmJ/FtsJ. *Biochem Biophys. Res Commun.* **271**, 714–718 (2000).
32. Ragheb, M. N. et al. Inhibiting the evolution of antibiotic resistance. *Mol. Cell* **73**, 157–165.e5 (2019).
33. Brauner, A., Fridman, O., Gefen, O. & Balaban, N. Q. Distinguishing between resistance, tolerance and persistence to antibiotic treatment. *Nat. Rev. Microbiol.* **14**, 320–330 (2016).
34. Nandy, P., Chib, S. & Seshasayee, A. A mutant RNA polymerase activates the general stress response, enabling *Escherichia coli* adaptation to late prolonged stationary phase. *mSphere* **5**, e00092–20 (2020).
35. Harms, A. et al. Adenylylation of gyrase and topo IV by FicT toxins disrupts bacterial DNA topology. *Cell Rep.* **12**, 1497–1507 (2015).
36. Norstrom, T., Lannergard, J. & Hughes, D. Genetic and phenotypic identification of fusidic acid-resistant mutants with the small-colony-variant phenotype in *Staphylococcus aureus*. *Antimicrob. Agents Chemother.* **51**, 4438–4446 (2007).
37. Pletnev, P. et al. Comprehensive Functional Analysis of *Escherichia coli* Ribosomal RNA Methyltransferases. *Front. Genet.* **11**, 472170 (2020).
38. Huang, C., Li, W. & Chen, J. Stringent response factor DksA contributes to fatty acid degradation function to influence cell membrane stability and polymyxin B resistance of *Yersinia enterocolitica*. *Int. J. Mol. Sci.* **24**, 11951 (2023).
39. Hurrell, E. et al. Neonatal enteral feeding tubes as loci for colonisation by members of the *Enterobacteriaceae*. *BMC Infect. Dis.* **9**, 146 (2009).
40. Ioannidis, A., Kyratsa, A., Ioannidou, V., Bersimis, S. & Chatzipanagiotou, S. Detection of biofilm production of *Yersinia enterocolitica* strains isolated from infected children and comparative antimicrobial susceptibility of biofilm versus planktonic forms. *Mol. Diag. Ther.* **18**, 309–314 (2014).
41. Horne, S. M. & Prüß, B. M. Global gene regulation in *Yersinia enterocolitica*: effect of FliA on the expression levels of flagellar and plasmid-encoded virulence genes. *Arch. Microbiol.* **185**, 115–126 (2006).

42. Lê-Bury, P., Echenique-Rivera, H., Pizarro-Cerdá, J. & Dussurget, O. Determinants of bacterial survival and proliferation in blood. *FEMS Microbiol Rev.* **48**, fuae013 (2024).

43. Cheng, Z. et al. Glycine, serine and threonine metabolism confounds efficacy of complement-mediated killing. *Nat. Commun.* **10**, 3325 (2019).

44. Kou, T. et al. Exogenous glycine promotes oxidation of glutathione and restores sensitivity of bacterial pathogens to serum-induced cell death. *Redox Biol.* **58**, 102512 (2022).

45. Proctor, R. A. et al. *Staphylococcus aureus* small colony variants (SCVs): a road map for the metabolic pathways involved in persistent infections. *Front Cell Infect. Microbiol* **4**, 99 (2014).

46. Das, S. et al. Natural mutations in a *Staphylococcus aureus* virulence regulator attenuate cytotoxicity but permit bacteremia and abscess formation. *Proc. Natl. Acad. Sci. USA* **113**, E3101–E3110 (2016).

47. Ding, X. et al. Airway environment drives the selection of quorum sensing mutants and promote *Staphylococcus aureus* chronic lifestyle. *Nat. Commun.* **14**, 8135 (2023).

48. Chau, N. Y. E., Ahmad, S., Whitney, J. C. & Coombes, B. K. Emerging and divergent roles of pyrophosphorylated nucleotides in bacterial physiology and pathogenesis. *PLoS Pathog.* **17**, e1009532 (2021).

49. Qi, W. et al. The effect of the stringent response and oxidative stress response on fitness costs of *de novo* acquisition of antibiotic resistance. *Int J. Mol. Sci.* **25**, 2582 (2024).

50. Chen, H. et al. Molecular turn in *Yersinia pestis* pathogenesis: implications of the *gppA* frameshift for bacterial survival in human macrophage. *Emerg. Microbes Infect.* **14**, 2467778 (2025).

51. Cantu, D. C., Chen, Y. & Reilly, P. J. Thioesterases: A new perspective based on their primary and tertiary structures. *Protein Sci.* **19**, 1281–1295 (2010).

52. Keita, A. K. et al. Resurgence of Ebola virus in 2021 in Guinea suggests a new paradigm for outbreaks. *Nature* **597**, 539–543 (2021).

53. Colangeli, R. et al. Whole genome sequencing of *Mycobacterium tuberculosis* reveals slow growth and low mutation rates during latent infections in humans. *PLoS One* **9**, e91024 (2014).

54. De Silva, K., Fife, A., Murgatroyd, F. & Gall, N. Pacemaker endocarditis: an important clinical entity. *BMJ Case Rep.* **2009**, bcr0220091608 (2009).

55. Le Guern, A. S., Martin, L., Savin, C. & Carniel, E. Yersiniosis in France: overview and potential sources of infection. *Int J. Infect. Dis.* **46**, 1–7 (2016).

56. Savin, C. et al. Genus-wide *Yersinia* core-genome multilocus sequence typing for species identification and strain characterization. *Microbiol. Genom.* **5**, e000301 (2019).

57. Seemann, T. Snippy: rapid haploid variant calling and core genome alignment. <https://github.com/tseemann/snippy> (2015).

58. Croucher, N. J. et al. Rapid phylogenetic analysis of large samples of recombinant bacterial whole genome sequences using Gubbins. *Nucleic Acids Res.* **43**, e15 (2015).

59. Minh, B. Q. et al. IQ-TREE 2: New models and efficient methods for phylogenetic inference in the genomic era. *Mol. Biol. Evol.* **37**, 1530–1534 (2020).

60. Letunic, I. & Bork, P. Interactive Tree Of Life (iTOL) v4: recent updates and new developments. *Nucleic Acids Res.* <https://doi.org/10.1093/nar/gkz239> (2019).

61. Yang, Z. PAML 4: phylogenetic analysis by maximum likelihood. *Mol. Biol. Evol.* **24**, 1586–1591 (2007).

62. Gautreau, G. et al. PPanGGOLiN: depicting microbial diversity via a partitioned pan-genome graph. *PLoS Comput. Biol.* **16**, e1007732 (2020).

63. Katoh, K. & Standley, D. M. MAFFT multiple sequence alignment software version 7: improvements in performance and usability. *Mol. Biol. Evol.* **30**, 772–780 (2013).

64. Nguyen, L. T., Schmidt, H. A., von Haeseler, A. & Minh, B. Q. IQ-TREE: a fast and effective stochastic algorithm for estimating maximum-likelihood phylogenies. *Mol. Biol. Evol.* **32**, 268–274 (2015).

65. Kalyaanamoorthy, S., Minh, B. Q., Wong, T. K. F., von Haeseler, A. & Jermiin, L. S. ModelFinder: fast model selection for accurate phylogenetic estimates. *Nat. Methods* **14**, 587–589 (2017).

66. Kaniga, K., Delor, I. & Cornelis, G. R. A wide-host-range suicide vector for improving reverse genetics in Gram-negative bacteria: inactivation of the *blaA* gene of *Yersinia enterocolitica*. *Gene* **109**, 137–141 (1991).

67. Narasimhan, M. L., Lampi, J. L. & Cronan, J. E. Genetic and biochemical characterization of an *Escherichia coli* K-12 mutant deficient in acyl-coenzyme A thioesterase II. *J. Bacteriol.* **165**, 911–917 (1986).

68. Wu, T. et al. clusterProfiler 4.0: A universal enrichment tool for interpreting omics data. *Innovation* **2**, 100141 (2021).

69. Binns, D. et al. QuickGO: a web-based tool for Gene Ontology searching. *Bioinformatics* **25**, 3045 (2009).

70. Perez-Riverol, Y. et al. The PRIDE database resources in 2022: a hub for mass spectrometry-based proteomics evidences. *Nucleic Acids Res.* **50**, D543–D552 (2022).

71. Lê-Bury, P. In-host evolution of *Yersinia enterocolitica* during a chronic human infection - R code. Zenodo <https://doi.org/10.5281/ZENODO.15526017> (2025).

Acknowledgements

This work was funded by Santé Publique France (SpF, Saint-Maurice, France - C.S., L.G., J.M., R.Beau, N.C., E.C. and J.P.-C), Institut Pasteur (C.S., P.L.-B., J.G., T.D., G.M.F., L.G., J.M., R.Beau, N.C., M.M., O.D., E.C. and J.P.-C), Direction Générale de l'Armement, Agence de l'Innovation de Défense (P.L.-B., G.M.F.), Fondation pour la Recherche Médicale (P.L.-B., FDT20220401-711 5222), the Inception program (P.L.-B., Investissement d'Avenir grant ANR-16-CONV-0005), ANRS Emerging Infectious Disease (P.L.-B., ANRS0349b) and Université Paris Cité (C.S., P.L.-B., J.G., T.D., G.M.F., L.G., J.M., R.Beau, N.C., M.M., O.D., E.C. and J.P.-C). The *Yersinia* Research Unit is a member of the LabEX IBEID (ANR-10LBX-62-IBEID - C.S., P.L.-B., G.M.F., L.G., J.M., R.Beau, N.C., O.D., E.C. and J.P.-C). We thank Vincent Enouf and Andreea Alexandru (P2M platform, Institut Pasteur, Paris, France) for the sequencing of the strains, Daniel Boury (SID'COM, University of Tours) for transesophageal echocardiography image processing, and Pr. Frédéric Patat (University Hospital of Tours) for transesophageal echocardiography image interpretation. Some figures were created with BioRender.

Author contributions

C.S. and P.L.-B. planned, performed and analyzed experiments with the help of N.C., L.G., J.M. and R.Beau. J.G. set up and performed pan-genome together with PAML analysis. G.M.F. calculated evolutionary rates and provided interpretation. R.Buzelé, C.L.-B., F.B., M.F. and B.B. are the physicians who took care of the patient and shared all the clinico-epidemiological data. L.D. performed antibiograms and MIC measurement. T.D. performed mass spectrometry-based proteomics. P.L.-B. and O.D. were involved in proteome analysis and identification of antibiotic tolerance mechanism. C.S., P.L.-B. and J.P.-C. interpreted data and wrote the manuscript. E.C., O.D., M. M., P.L. and J.P.-C. supervised the work. C.S. and P.L.-B. are shared first authors and P.L. and J.P.-C. are shared last authors.

Competing interests

The authors declare no competing interests.

Inclusion & Ethics Statement

All collaborators of this study have fulfilled the criteria for authorship required by Nature Portfolio journals. Roles and responsibilities were agreed among collaborators ahead of the research. This research was

not severely restricted or prohibited in the setting of the researchers, and does not result in stigmatization, incrimination, discrimination, or personal risk to participants. The ethical committee of the University Hospital of Tours was informed about the study. The study is registered under the number 2025-032.

Additional information

Supplementary information The online version contains supplementary material available at
<https://doi.org/10.1038/s41467-025-60782-6>.

Correspondence and requests for materials should be addressed to Cyril Savin or Javier Pizarro-Cerdá.

Peer review information *Nature Communications* thanks Mikael Skurnik, Oleksandr Maistrenko, and the other, anonymous, reviewer(s) for their contribution to the peer review of this work. A peer review file is available.

Reprints and permissions information is available at
<http://www.nature.com/reprints>

Publisher's note Springer Nature remains neutral with regard to jurisdictional claims in published maps and institutional affiliations.

Open Access This article is licensed under a Creative Commons Attribution-NonCommercial-NoDerivatives 4.0 International License, which permits any non-commercial use, sharing, distribution and reproduction in any medium or format, as long as you give appropriate credit to the original author(s) and the source, provide a link to the Creative Commons licence, and indicate if you modified the licensed material. You do not have permission under this licence to share adapted material derived from this article or parts of it. The images or other third party material in this article are included in the article's Creative Commons licence, unless indicated otherwise in a credit line to the material. If material is not included in the article's Creative Commons licence and your intended use is not permitted by statutory regulation or exceeds the permitted use, you will need to obtain permission directly from the copyright holder. To view a copy of this licence, visit <http://creativecommons.org/licenses/by-nc-nd/4.0/>.

© The Author(s) 2025